DEPARTMENT OF CIVIL ENGINEERING

UNIVERSITY OF SOUTHERN CALIFORNIA

FREQUENCY DEPENDENT ATTENUATION OF STRONG EARTHQUAKE GROUND MOTION

by

M. D. Trifunac and V. W. Lee

Report No. CE 85-02

Los Angeles, California

October, 1985

ABSTRACT

New frequency dependent attenuation function of Fourier amplitude spectra of recorded strong earthquake ground acceleration has been developed. The iterative regression analyses assume simple functional forms to model the trends of the data and have sufficient flexibility to detect dependence of attenuation on source dimensions, depth and frequency of wave motion. It has been found that for distances less than about 100 km there is clear frequency dependent variation of attenuation functions, with high frequency amplitudes attenuating faster with distance.

The strong motion data recorded so far is not adequate to describe attenuation of strong motion amplitudes for distances greater than about 150 km. To facilitate approximate characterization of attenuation of strong motion amplitudes for these and for larger distances it has been proposed to use the attenuation function developed by Richter for the computation of local magnitude scale in Southern California.

INTRODUCTION

Some fifty years ago (March 10, 1933) the first strong motion accelerogram was recorded during the Long Beach, California, earthquake (Hudson, 1983). Following this event the strong motion accelerograph network in California grew through the 1940's, 1950's and the first part of the 1960's. Beginning in the late 1960's the number of accelerograph stations began to increase more rapidly as a result of numerous specialized observational projects and the expansion of the strong-motion network from California into the Central and Eastern United States. At present there are numerous strong motion stations permanently installed on ground sites, dams, bridges, buildings, nuclear power plants, in specially designed arrays along major active faults and in large arrays in metropolitan Los Angeles and San Francisco areas (Hudson 1983).

Following the San Fernando, California, earthquake of 1971, the digitized and uniformly processed strong motion accelerograph data base has grown to a point where it became possible to initiate studies of the dependence of the characteristics of recorded motions on earthquake size, nature of the wave propagation path and the local recording site conditions. In many of these analyses it has been essential to include a description of wave amplitude attenuation with distance, either to compare various inferences at a chosen convenient distance or to be able to interpolate or extrapolate outside the available data range. Analysis of various published attenuation relations shows that those could be grouped roughly into 1) Empirical attenuation laws and 2) Pseudo analytical attenuation laws. The empirical attenuation laws have aimed to exploit the available seismological data and experience and to modify

and extend largely "distant" attenuation laws to "smaller" near source distances. Examples of uses of such attenuation laws are those employed by Gutenberg and Richter (1942, 1956) and by Trifunac (1976a, b) who used the Richter's attenuation function developed for the calculation of local magnitude scale M_L, in Southern California. With few exceptions most "analytical" attenuation laws take a form which tends to a constant for small source to station distance and decays like a power of distance for large distances. The majority of published attenuation studies fall into this latter category (e.g., Trifunac and Brady 1975, Nuttli and Herrmann 1981).

With the development of extended source representations, through the studies of finite earthquake source dislocations analytically (e.g., De Hoop, 1958; Haskell, 1969; Aki and Richards, 1980) and observation of recorded accelerograms (e.g., Trifunac 1972, 1974) it became possible to understand better the physical nature of attenuation near extended earthquake sources. Thus following Haskell (1969), for example, it is seen that the strong earthquake ground motion consists of waves which in elastic medium attenuate like $1/R^4$, $1/R^2$, $1/R$ and $1/R^{\frac{1}{2}}$. The distance ranges where these attenuation rates dominate will vary and will depend on the source mechanism, source size and depth, complexity of the surrounding geological medium and on its inelastic attenuation properties. In Sourthern California at a distance of about 100 km the surface waves begin to dominate in the recorded motions. At distances less than about 100 km the orientation, the size and the shape of the fault surface, influence the shape of the overall attenuation law of wave amplitudes. At small distances the near field effects integrated over the fault surface will tend to diminish the wave attenuation for larger faults.

At comparable distances the small dislocation surfaces will progressively look more like point sources and thus will lead to more rapid attenuation of wave amplitudes with distance. For points vary close to the causative fault the strong motion amplitudes will primarily depend on the stress released during faulting and the resulting permanent displacement in short and long period motions respectively, while the overall source size will cease to be significant when it exceeds certain characteristic source dimension. Consequently, close to the source the strong motion amplitudes will grow only weakly with the overall source size and this rate of growth will be noticeable only for source dimensions smaller than certain characteristic fault size. For larger faults this rate of growth should essentially go to zero. Thus the shapes of the strong motion attenuation curves will change with source dimensions. For distances, large enough, most sources will lead to parallel attenuation curves (i.e., no size dependent slopes) governed mainly by surface wave attenuation. For smaller distances the smaller earthquakes will lead to steeper attenuation curves so that a family of different attenuation curves for different magnitudes will tend to "converge" closer to each other as the observation point moves closer to the source. The relative separation of different attenuation curves will tend to be constant and grow with earthquake size at a constant rate for large distances. The same separation and its rate of growth near a fault will, at first, be small and then will disapear with increasing source dimensions.

The foregoing qualitative expectations have been known to many researchers. The difficulty lies in the lack of sufficient data for their

quantitative evaluation. The aim of this work is to address this quantitative aspect by trying to work with data available so far.
In this process numerous, physical and geometrical characteristics of earthquake sources will have to be ignored. Otherwise the effort would not be feasible or the data base would become inadequate. Such effects as radiation pattern, directivity, fault type, stress drop, and seismic moment, to name a few, will be ignored. To this end we will assume that the small perturbations of recorded motions, up or down, by less than the equivalent of one half magnitude unit will not alter the "raw data nature" of recorded motions. In the following we outline how this perturbation to the data has been performed, and present our proposal for describing the frequency dependent attenuation curves of strong motion amplitudes with distance.

FREQUENCY DEPENDENT ATTENUATION FUNCTION

1. Previous Analysis

During the regression analyses of earthquake strong-motion parameters in the 1970's, it was suggested that the peaks of strong ground motion might be scaled by using the following expression (Trifunac and Brady, 1975)

$$\log_{10}\begin{Bmatrix} a_{max} \\ v_{max} \\ d_{max} \end{Bmatrix} = M + \log_{10}A_o(R) - \log_{10}\begin{Bmatrix} a_o(M) \\ v_o(M) \\ d_o(M) \end{Bmatrix}, \qquad (1.1)$$

where a_{max}, v_{max} and d_{max} represent respectively, the peak acceleration, peak velocity and peak displacement amplitudes; M is the local earthquake magnitude, M_L; $\log_{10}A_o(R)$ represents the amplitude attenuation function (Richter, 1958) versus distance (Table 1.1). It is empirically determined for Southern California and representative of wave frequencies centered near the middle of the frequency band for the data used in the regression of strong motion acceleration (0.1 Hz to 25 Hz). $a_o(M)$, $v_o(M)$ and $d_o(M)$ are respectively the magnitude-dependent empirical scaling functions for acceleration, velocity and displacement.

Trifunac (1976b) generalized the above regression analysis to the study of Fourier Amplitude Spectra. The same empirical model was applied to the scaling of spectral amplitudes at a selected set of discrete periods, T. For this purpose, (1.1) was generalized to become (equation (2) in Trifunac (1976b))

$$\log_{10}[FS(T),_p] = M + \log_{10}A_o(R) - \log_{10}\{FS_o(T,M,p,s,v,R)\} \qquad (1.2)$$

Table 1.1 $\log_{10}A_o(R)$ vs epicentral distance R

R(km)	$-\log_{10}A_o(R)$	R(km)	$-\log_{10}A_o(R)$	R(km)	$-\log_{10}A_o(R)$
1	1.400	140	3.230	370	4.336
5	1.500	150	3.279	380	4.376
10	1.605	160	3.328	390	4.414
15	1.716	170	3.378	400	4.451
20	1.833	180	3.429	410	4.485
25	1.955	190	3.480	420	4.518
30	2.078	200	3.530	430	4.549
35	2.199	210	3.581	440	4.579
40	2.314	220	3.631	450	4.607
45	2.421	230	3.680	460	4.634
50	2.517	240	3.729	470	4.660
55	2.603	250	3.779	480	4.685
60	2.679	260	3.827	490	4.709
65	2.746	270	3.877	500	4.732
70	2.805	280	3.926	510	4.755
80	2.920	290	3.975	520	4.776
85	2.958	300	4.024	530	4.797
90	2.989	310	4.072	540	4.817
95	3.020	320	4.119	550	4.835
100	3.044	330	4.164	560	4.853
110	3.089	340	4.209	570	4.869
120	3.135	350	4.253	580	4.885
130	3.182	360	4.295	590	4.900

where M is earthquake magnitude, $\log_{10}A_o(R)$ is the same attenuation function that was used in (1.1), p is the confidence level selected for the approximate bound of spectral amplitudes $FS(T)_{,p}$, s represents the type of site conditions (s=0 for alluvium, s=1 for intermediate rocks, and s=2 for basement rocks), v designates the horizontal or vertical components (v=0 for horizontal, v=1 for vertical), and $FS_o(T,M,p,s,v,R)$ represents an empirical scaling function to be determined by regression analysis. The same empirical model was also used for scaling of absolute acceleration spectra, SA (Trifunac and Anderson, 1977), pseudo relative velocity spectra PSV (Trifunac and Anderson, 1978a) and relative velocity spectra, SV (Trifunac and Anderson, 1978b).

Trifunac and Lee (1978) refined the above analyses by introducing a measure of the depth of sedimentary deposits, h, as a site characteristic (instead of s used above). The new scaling equation then becomes

$$\log_{10}[FS(T)] = M + \log_{10}A_o(R) - b(T)M - c(T) - d(T)h - e(T)v - f(T)M^2 - g(T)R \qquad (1.3)$$

with all the other parameters defined as before. The functions b(T), c(T), ... and g(T) are estimated by regression analysis at 91 periods T between 0.04 sec and 15 sec. The form g(T)R in (1.3) models the period-dependent attenuation "correction factor" for distance R in addition to the attenuation function $\log A_o(R)$. Its form corresponds to the usual amplitude attenuation $\exp(-\pi R/Q\beta T)$, on a linear scale, employed to model approximately the effects of anelastic attenuation. Here β is the shear wave velocity and Q the attenuation constant. In (1.3), g(T) may then be thought of as corresponding to $(\pi/Q\beta T)\log_{10}e$,

if it is assumed that the $\log_{10}A_o(R)$ term represents the geometric spreading only. The $\log_{10}A_o(R)$ has been derived empirically from data on actual peak amplitudes in Southern California, (Richter, 1958) and thus represents an average combination of geometric spreading and an elastic attenuation for a frequency band around 1 Hz. The term g(T)R can then only represent a correction to the average attenuation, $\log_{10}A_o(R)$.

2. Limitations of the $\log_{10}A_o(R)$ Function

The physical significance of $\log_{10}A_o(R)$ lies in its sound data base gathered for numerous earthquake observations in Southern California. It is characterized well by defining a corresponding new function which is given by (Trifunac, 1976a) as

$$f(R) = \log_{10}A_o(0) - \log_{10}A_o(R) \ . \tag{1.4}$$

f(R) can be approximated by two straight line segments which are

$$f(R) = \begin{cases} R/50 & R \leq 75 \text{ km} \\ 1.125 + R/200 & 75 \leq R \leq 350 \text{ km} \ . \end{cases} \tag{1.5}$$

The change in slope at R = 75 km suggests that at large distances ($R \geq 75$ km), the main contribution to strong shaking comes from surface waves.

The advantage in using the $\log_{10}A_o(R)$ function is that it contains information on the average properties of wave propagation through the crust in Southern California, where virtually all strong motion data have been recorded up to and during the 70's. The disadvantages and

limitations, however, which result from using $\log_{10}A_o(R)$ in previous regression analyses are that its shape does not depend on magnitude, i.e., source dimension of an earthquake, on the focal depth of an earthquake, on the geological environment of the recording station, or on the actual amplitudes of recorded motions. That $\log_{10}A_o(R)$ or its analog should depend on the geometric size of the fault has been discussed in some detail previously (Trifunac, 1976b). These magnitude dependent changes of $\log_{10}A_o(R)$ would be such that for small R the slope of $\log_{10}A_o(R)$ would tend to be steeper for earthquakes with small fault dimensions, while for large faults and for small R, $\log_{10}A_o(R)$ would tend to flatten out and have a smaller slope than the average function. Through the 1970's only a few of the 186 records available for analysis had epicentral distances less than 10 km. The empirical derivation of different shapes of $\log_{10}A_o(R)$, or its equivalent, for different magnitudes or source dimensions then did not seem feasible.

3. The New Database

Through the years new earthquake acceleration data are added to the original data base. The list of 57 earthquakes which we used through the 1970's has now grown to a list of 104 earthquakes most of which occurred mainly in the regions of northern and southern California. Table 3.1 is the list of earthquakes now used in our database. Each line contains the date and time of the earthquake, magnitude, location of the epicenter, focal depth and maximum intensity, if available, and the name of the earthquake.

TABLE 3.1

EQ #	MON	DAY	YR	TIME CODE	LATITUDE DEG, MIN & SEC	LONGTITUDE DEG, MIN & SEC	DEPTH (KM)	MAG	MAX MMI	NAME
1	3	10	1933	1754PST	33 37 00	-117 58 00	16.0	6.3	9	LONG BEACH, CALIF
2	10	2	1933	0110PST	33 47 00	-118 08 00	16.0	5.4	6	SOUTHERN CALIF
3	7	6	1934	1449PST	41 42 00	-124 36 00			5	EUREKA, CALIF
4	12	30	1934	0552PST	32 15 00	-115 30 00	16.0	6.5	9	LOWER CALIF
5	10	31	1935	1138MST	46 37 00	-111 58 00		6.0	8	HELENA, MT
6	10	31	1935	1218MST	46 37 00	-111 58 00			3	HELENA, MT
7	11	21	1935	2058MST	46 36 00	-112 00 00			6	HELENA, MT
8	11	28	1935	0742MST	46 37 00	-111 58 00			6	HELENA, MT
9	2	6	1937	2042PST	40 30 00	-125 15 00			5	HUMBOLDT BAY, CAL
10	4	12	1938	0825PST	32 53 00	-115 35 00	16.0	3.0		IMPERIAL VALLEY, CA
11	6	5	1938	1842PST	32 54 00	-115 13 00	16.0	5.0		IMPERIAL VALLEY, CA
12	6	6	1938	0435PST	32 15 00	-115 10 00	16.0	4.0		IMPERIAL VALLEY, CA
13	9	11	1938	2210PST	40 18 00	-124 48 00		5.5	6	NW CALIF
14	5	18	1940	2037PST	32 44 00	-115 30 00	16.0	6.7	10	IMPERIAL VALLEY, CA
15	2	9	1941	0145PST	40 42 00	-125 24 00		6.4		NW CALIF
16	6	30	1941	2351PST	34 22 00	-119 35 00	16.0	5.9	8	SANTA BARBARA, CAL
17	10	3	1941	0813PST	40 36 00	-124 36 00		6.4	7	NORTHERN CALIF
18	11	14	1941	0042PST	33 47 00	-118 15 00	16.0	5.4	8	TORRANCE-GARDENA CA
19	10	21	1942	0822PST	32 58 00	-116 00 00	16.0	6.5	7	BORREGO VALLEY, CAL
20	3	9	1949	0429PST	37 06 00	-121 18 00		5.3	7	NORTHERN CALIF
21	4	13	1949	1156PST	47 06 00	-122 42 00		7.1	8	WESTERN WASH
22	1	23	1951	2317PST	32 59 00	-115 44 00	16.0	5.6	7	IMPERIAL VALLEY, CA
23	10	7	1951	2011PST	40 17 00	-124 48 00		5.8	7	NW CALIF
24	7	21	1952	0453PDT	35 00 00	-119 01 00	16.0	7.7	11	KERN COUNTY, CALIF
25	7	23	1952		35 17 00	-118 39 00				KERN CNTY, CAL
26	9	22	1952	0441PDT	40 12 00	-124 25 00		5.5	7	NORTHERN CALIF
27	11	21	1952	2346PST	35 50 00	-121 10 00		6.0	7	SOUTHERN CALIF
28	6	13	1953	2017PST	32 57 00	-115 43 00	16.0	5.5	7	IMPERIAL VALLEY, CA
29	1	12	1954	1534PST	35 00 00	-119 01 00	16.0	5.9	8	WHEELER RIDGE, CALI
30	4	25	1954	1233PST	36 48 00	-121 48 00		5.3	7	CENTRAL CALIF
31	11	12	1954	0427PST	31 30 00	-116 00 00	16.0	6.3	5	LOWER CALIF
32	12	21	1954	1156PST	40 47 00	-123 52 00		6.5	7	EUREKA, CALIF
33	9	4	1955	1801PST	37 22 00	-121 47 00		5.8	7	SAN JOSE, CALIF
34	12	16	1955	2117PST	33 00 00	-115 30 00	16.0	4.3		IMPERIAL COUNTY, CA
35	12	16	1955	2142PST	33 00 00	-115 30 00	16.0	3.9		IMPERIAL COUNTY, CA
36	12	16	1955	2207PST	33 00 00	-115 30 00	16.0	5.4	7	IMPERIAL COUNTY
37	2	9	1956	0633PST	31 42 00	-115 54 00	16.0	6.8		EL ALAMO, BAJA CAL
38	2	9	1956	0725PST	31 42 00	-115 54 00		6.4		EL ALAMO, BAJA CAL
39	3	18	1957	1056PST	34 07 06	-119 13 12	13.8	4.7	6	SOUTHERN CALIF
40	3	22	1957	1048PST	37 40 00	-122 28 00		3.8	5	SAN FRANCISCO CA
41	3	22	1957	1144PST	37 40 00	-122 29 00		5.3	7	SAN FRANCISCO, CAL
42	3	22	1957	1515PST	37 39 00	-122 27 00		4.4	5	SAN FRANCISCO CA
43	3	22	1957	1627PST	37 39 00	-122 29 00		4.0	5	SAN FRANCISCO CA
44	1	19	1960	1926PST	36 47 00	-121 26 00		5.0	6	CENTRAL CALIF
45	6	5	1960	1718PST	40 49 00	-124 53 00		5.7	6	NORTHERN CALIF
46	4	8	1961	2323PST	36 30 00	-121 18 00	11.0	5.7	7	HOLLISTER, CALIF
47	9	4	1962	0917PST	40 58 00	-124 12 00		5.0	6	NORTHERN CALIF
48	4	29	1965	0729PST	47 24 00	-122 18 00		6.5	8	PUGET SOUND, WASH
49	7	15	1965	2346PST	34 29 06	-118 31 18	15.1	4.0	6	SOUTHERN CALIF
50	6	27	1966	2026PST	35 57 18	-120 29 54	6.0	5.6	7	PARKFIELD, CALIF
51	8	7	1966	0936PST	31 48 00	-114 30 00	16.0	6.3	6	GULF OF CALIF
52	9	12	1966	0841PST	39 24 00	-120 06 00		6.3	7	NORTHERN CALIF
53	12	10	1967	0407PST	40 30 00	-124 36 00		5.8	6	NORTHERN CALIF

54	12	18	1967	0925PST	37	00	36	-121	47	18		5.2	6	NORTHERN CALIF
55	4	8	1968	1830PST	33	11	24	-116	07	42	11.1	6.4	7	BORREGO MTN, CALIF
56	9	12	1970	0630PST	34	16	12	-117	32	24	8.0	5.4	7	LYTLE CREEK, CALIF
57	2	9	1971	0600PST	34	24	42	-118	24	00	13.0	6.4	11	SAN FERNANDO, CALIF
58	10	15	1979	1417PST	32	37	59	-115	19	59	12.0	6.6		IMPERIAL VALLEY, CA
59	8	6	1979	0805PST	37	06	43	-121	31	59	9.6	5.9		COYOTE LAKE, CALIF
60	8	13	1978	2254GMT	34	21	04	-119	42	00	12.5	5.5		SANTA BARBARA, CAL
61	1	24	1980	1100PST	37	49	37	-121	47	13	5.9	5.9		MT. DIABLO, LIVERMO
62	1	26	1980	1833PST	37	45	00	-121	42	47	7.3	5.2		MT. DIABLO, LIVERMO
63	08	02	1975	2022GMT	39	26	58	-121	28	25	4.1	5.2		OROVILLE AFTERSHOCK
64	08	02	1975	2059GMT	39	26	00	-121	28	31	5.1	5.2		OROVILLE AFTERSHOCK
65	08	03	1975	0103GMT	39	29	19	-121	30	59	8.8	4.6		OROVILLE AFTERSHOCK
66	08	03	1975	0247GMT	39	28	52	-121	30	21	7.4	4.1		OROVILLE AFTERSHOCK
67	08	05	1975	0228GMT	39	24	18	-121	29	43	6.2	3.2		OROVILLE AFTERSHOCK
68	08	06	1975	0350GMT	39	29	46	-121	31	49	9.2	4.7		OROVILLE AFTERSHOCK
69	08	06	1975	1641GMT	39	29	31	-121	31	45	9.7	3.9		OROVILLE AFTERSHOCK
70	08	08	1975	0700GMT	39	29	50	-121	30	41	7.7	4.8		OROVILLE AFTERSHOCK
71	08	11	1975	0611GMT	39	27	29	-121	28	59	3.1	4.4		OROVILLE AFTERSHOCK
72	08	11	1975	1559GMT	39	30	20	-121	31	35	9.8	3.8		OROVILLE AFTERSHOCK
73	08	16	1975	0548GMT	39	28	12	-121	31	42	8.5	4.1		OROVILLE AFTERSHOCK
74	08	16	1975	1223GMT	39	29	52	-121	30	16	7.1	3.1		OROVILLE AFTERSHOCK
75	09	27	1975	2234GMT	39	31	12	-121	31	56	10.4	4.6		OROVILLE AFTERSHOCK
76	11	28	1974	2301GMT	36	54	0	-121	30	0	9.0	0.	6	HOLLISTER, CAL
77	1	11	1975	1737PST	40	13	12	-124	15	36	2.0	4.7	6	NORTHERN CAL
78	5	6	1975	1835PST	40	16	48	-124	40	12	0.	4.0		NORTHERN CAL
79	6	7	1975	0846GMT	40	34	12	-124	08	24	21.0	5.7	7	NORTHERN CAL
80	3	8	1971	1508PST	35	40	0	-118	24	12	6.0	4.7	5	CENTRAL CAL
81	5	2	1971	0608GMT	51	24	0	-177	12	0	43.0	7.1	6	ANDREANOF, ALASKA
82	9	12	1971	1132PST	41	17	54	-123	40	24	20.0	4.6	5	NORTHERN CAL
83	7	30	1972	2145GMT	56	49	12	-135	40	48	25.0	7.1	7	SOUTHEAST ALASKA
84	9	4	1972	1804GMT	36	38	13	-121	17	13	2.0	4.8	6	CENTRAL CAL
85	5	26	1980	1857GMT	37	32	37	-118	51	41	2.8	4.9		MAMMOTH AFTERSHOCK
86	5	27	1980	1450GMT	37	27	49	-118	49	24	2.4	6.3		MAMMOTH AFTERSHOCK
87	5	27	1980	1901GMT	37	36	15	-118	46	11	3.8	5.0		MAMMOTH AFTERSHOCK
88	5	28	1980	0516GMT	37	34	49	-118	53	09	3.3	4.8		MAMMOTH AFTERSHOCK
89	5	31	1980	1516GMT	37	32	22	-118	54	22	8.2	5.1		MAMMOTH AFTERSHOCK
90	6	11	1980	0441GMT	37	30	24	-119	02	34	14.1	5.0		MAMMOTH AFTERSHOCK
91	6	28	1980	0058GMT	37	33	23	-118	51	45	5.1	4.1		MAMMOTH AFTERSHOCK
92	10	16	1979	1616PDT	33	4	29	-115	33	16	5.0	4.9		IMPERIAL VALLEY AFT
93	10	16	1979	1445PDT	33	2	44	-115	29	24	3.9	4.6		IMPERIAL VALLEY AFT
94	10	16	1979	1114PDT	32	58	19	-115	36	22	4.7	4.2		IMPERIAL VALLEY AFT
95	10	15	1979	2319GMT	32	46	0	-115	26	29	9.5	5.0		IMPERIAL VALLEY AFT
96	4	26	1981	1209GMT	33	7	48	-115	39	0	8.0	5.6		WESTMORELAND, CAL
97	1	24	1980	1900GMT	37	50	24	-121	48	0	5.9	5.9		LIVERMORE, CAL
98	1	26	1980	0233GMT	37	45	36	-121	42	0	7.3	5.2		LIVERMORE, CAL
99	5	25	1980	0934PDT	37	36	32	-118	50	49	9.0	6.1		MAMMOTH AFTERSHOCK
100	5	25	1980	0949PDT	37	37	41	-118	55	37	14.	6.0		MAMMOTH AFTERSHOCK
101	5	25	1980	1245PDT	37	33	40	-118	49	52	16.	6.1		MAMMOTH AFTERSHOCK
102	5	25	1980	1336PDT	37	37	30	-118	51	32	2.	5.7		MAMMOTH AFTERSHOCK
103	5	26	1980	1158PDT	37	32	35	-118	53	17	5.	5.7		MAMMOTH AFTERSHOCK
104	5	27	1980	0751PDT	37	30	22	-118	49	34	14.	6.2		MAMMOTH AFTERSHOCK

The original list of 186 free-field records corresponding to the 57 earthquakes has now grown to 438 free-field records from the total of 104 earthquakes. With 3 components available for each record, this amounts to a total of 1314 acceleration components, of which there are 876 horizontal and 438 vertical components.

4. The New Attenuation Function: Models I, II, III and IV

With the new database now available, the attenuation function which is to replace the Richter's $\log_{10}A_o(R)$ function can next be investigated. Four different models of this function have been studied and will be presented here. All four models assume that the attenuation function, should depend, on the distance, R, on the focal depth, H, and on the "size" of the fault, S. A parameter, Δ, is introduced in each model to replace the distance, R. Models III and IV will also have the attenuation function dependent on the coherence "length", S_o, at the fault (Gusev, 1983). Thus

$$\Delta = \Delta(R, H, S) \qquad \text{for models I and II ,}$$

$$\text{and} \qquad \Delta = \Delta(R,H,S,S_o) \qquad \text{for models III and IV .} \qquad (4.1)$$

(a) Model I

Model I defines Δ as

$$\Delta = (R^2 + H^2 + S^2)^{\frac{1}{2}} . \qquad (4.2)$$

Δ is thus used as a parameter to measure the "representative distance" from the earthquake source of size S, at depth H and distance R. Since the "fault size," S, is not available for most of the earthquakes used in the database, an empirical formula for the size has been introduced

for this and for all subsequent models (II, III and IV) of the attenuation function. It is defined as a function of the magnitude and period of the spectral amplitudes considered, so that

$$\text{size,} \quad S = S(M,T) \ , \tag{4.3}$$

and at each period T, the size of fault "felt" at that period is assumed to be a linear function of magnitude, M, so that

$$\begin{aligned} &\text{for} && M = 3 \ , && S = 0.2 \text{ km} \\ &\text{and} && M = 6.5 \ , && S = S_{6.5}(T) \text{ km} \end{aligned} \tag{4.4}$$

where $S_{6.5}(T)$ is an empirically determined function of period T for each model. The attenuation function, denoted by $\mathscr{A}tt(\Delta,M,T)$, will then be defined as

$$\mathscr{A}tt(\Delta,M,T) = \mathscr{A}_0(T)\log_{10}\Delta, \tag{4.5}$$

where $\mathscr{A}_0(T)$ will be an empirically determined function of period T for each model.

(b) Model II

Model I assumes that the "size" of the fault S = S(M,T), as defined in equation (4.3), is "felt" at the site independent of how close the site is to the earthquake source. It is reasonable to assume that if the site is "far enough," relative to the size of the fault, that the site will "see" the complete fault. It may be questionable, however, to assume the same to be true for sites at small and zero distances from the fault. For this reason we consider a modified definition of the fault size which approximately models this as follows:

$$S = \hat{S}(M,R,T)$$
$$= S(M,T)(1.-\exp(\ell n(.1)R/S(M,T)), \qquad (4.6)$$

with the factor, $(1.-\exp(\ell n(.1)R/S(M,T))$, multiplying the original definition of the fault size, S(M,T), in (4.3). This factor has been chosen with the property that at the epicenter where R=0, it is zero, so that the size of the fault "felt" is zero. Out at the epicentral distance equal to that of the fault size, that is, when R = S(M,T), this factor is .9, which means that 90% of the fault size if "felt." Beyond this distance, the factor asymptotically approaches 1, so that practically the whole fault size is "felt" for $R \gg S(M,T)$.

(c) Model III

Gusev (1983) investigated a descriptive statistical model of earthquake source radiation and applied this model to an estimation of short-period strong earthquake ground motion. He considered a concept of a subsource, as an element of the main rupture process. The source radiation is then described by overlapping the source functions and radiation pulses of the subsources of different sizes. The correlation radius, S_o, of the source function can be approximated by one half of the wavelength λ in a frequency band around f, namely

$$\text{correlation radius,} \quad S_o \approx \lambda/2 = C_s/2f = C_sT/2 \qquad (4.7)$$

where C_s is the shear wave velocity. Then following Gusev (1983) we consider a definition of a "representative distance" from the earthquake source of size S, at depth H and at distance R to the site as

$$\Delta = S\left(\ell n \frac{R^2 + H^2 + S^2}{R^2 + H^2 + S_o^2}\right)^{-\frac{1}{2}}$$

This expression has the property that when $S^2 << R^2 + H^2$, it asymptotically approaches $(R^2 + H^2)^{\frac{1}{2}}$, the distance between the focus and the site. Using:

$$\ell n(1 + x) = x - \frac{x^2}{2} + \frac{x^3}{3} - \frac{x^4}{4} + \ldots \tag{4.9}$$

in (4.8)

$$\ell n \frac{R^2 + H^2 + S^2}{R^2 + H^2 + S_o^2} \sim \frac{S^2}{R^2 + H^2} (1 - (S_o/S)^2) \ . \tag{4.10}$$

When $S^2 << R^2 + H^2$, (4.8) gives

$$\Delta \sim \sqrt{(R^2+H^2)/(1 -(S_o/S)^2)}. \tag{4.11}$$

At high frequencies, $T \sim 0$, and $S_o \sim 0$ from (4.7), so that the representative distance Δ becomes $R^2 + H^2$ when $R^2 + H^2 >> S^2$.

(d) Model IV

As in model I, the expression for Δ in Model III assumed that the "size" of the fault $S = S(M,T)$ that is "felt" at the site is independent of how close the site is to the earthquake source. Following the ideas discussed in the description of Model II, to reduce the size of the fault "felt" at distances close to the fault, we consider yet another description of the fault size as follows:

$$\hat{S} = \min\{S,(R^2 + H^2)^{\frac{1}{2}}\}, \tag{4.12}$$

so that at distances smaller than the size of the fault, S, the size of the fault "felt", $\hat{S}$, is set to be equal to the hypocentral distance, $(R^2 + H^2)^{\frac{1}{2}}$.

The new definition of the "representative" distance Δ then takes the form

$$\Delta = \hat{S}\left(\ell n \frac{R^2 + H^2 + \hat{S}^2}{R^2 + H^2 + S_o^2}\right)^{\frac{1}{2}} \tag{4.13}$$

5. Determination of Attenuation Functions

The following is a description of the procedures we employed to determine the frequency dependent attenuation function for each of the four models described above.

Step 1: We started with the regression equation of Fourier Spectral Amplitudes:

$$\log_{10}FS(T) = M + \mathscr{A}tt(\Delta,M.T) + b_1(T)M + b_2(T)h + b_3(T)v + b_4(T)\Delta/100 + b_5(T) + b_6(T)M^2 \quad (5.1)$$

where $\mathscr{A}tt(\Delta,M,T)$ is the new attenuation function to be determined for each of the four models. In the first iteration $\mathscr{A}tt(\Delta,M,T)$ was taken to be $\log_{10}A_o(\Delta)$, the Richter's attenuation function, with the parameter Δ equal to R. Using (5.1), a regression analysis is performed on the new database of 1314 components of Fourier spectrum amplitude data FS(T), at 91 discrete periods T ranging from 0.04 to 15.0 sec. This first step is identical to the regression analyses used for the old database (Trifunac, 1976a,b; Trifunac and Lee, 1978). As before, the data are screened to minimize possible bias in the model. This could result from uneven distribution of data among the different magnitude ranges and from excessive contribution to the database from several abundantly recorded earthquakes. To carry out the screening the data are partitioned into six groups corresponding to magnitude ranges: 2.0-2.9, 3.0-3.9, 4.0-4.9, 5.0-5.9, 6.0-6.9 and 7.0-7.9. The data in each of these magnitude ranges are next subdivided according to the site classifications s=0,1 and 2. The data within each of these

subgroups were then divided into 2 sets corresponding to horizontal (v=0) and vertical (v=1) components. The resulting data in each of the groups corresponds to the Fourier spectral amplitudes from a specified earthquake magnitude range for a specified site classification and with specified component orientation. To study the effect of attenuation at large distances, the data in each of the subgroups are subdivided further into 2 sets: one for epicentral distances $\leq$ 100 km and the other for distances > 100 km. The data in each of these two final subsets are then arranged in monotonically increasing order in terms of their amplitudes. If the number of data points in the first set ($R \leq 100$ km) is less than 19, all the data points are taken. If there are more than 19 points in this first set, at most 19 points are selected from among the ordered set of data so that they correspond uniformly, as close as possible, to the 5% , 10%, ... , 90% and 95% percentiles at distances $R \leq 100$ km. Similarly, at most 5 points are selected from the second set ($R > 100$ km) of data so that those correspond uniformly to around 16 2/3%, 33 1/3%, 50%, 66 2/3% and 83 1/3% percentiles at distances $R > 100$ km. This approximate scheme has the effect of reducing the bias described above. The resulting fitted coefficients at each period T resulting from linear regression will be denoted by $\hat{b}_1(T)$, $\hat{b}_2(T)$, $\hat{b}_3(T)$, $\hat{b}_4(T)$, $\hat{b}_5(T)$ and $\hat{b}_6(T)$, (equation (5.1).

Step 2: With the regression coefficients available from Step 1, a modified set of Fourier amplitudes is next prepared from the original database of 1314 records. The database of modified Fourier Spectral Amplitudes, MFS(T), is to consist of data for the same sites with the

same input parameter Δ, but with the depth of sediments modified to h = 2 km, the component parameter to v = 0 (horizontal), and is to correspond to one of the closest magnitudes from among the list:

2.5, 3.0, 3.5, 4.0, 4.5, 5.0, 5.5, 6.0, 6.5, 7.0. 7.5, 8.0 .

The resulting database will then consist of data from sites all with the same alluvial depth (h = 2 km), the same component orientation (v = 0) and one of the above discrete magnitude values. For example, if the original Fourier Spectrum Amplitude, FS(T) is available at a site from an earthquake of magnitude 6.3, the closest magnitude from among the list would be 6.5. The modified Fourier Spectrum Amplitude, MFS(T) would then be calculated from

$$\log_{10}\mathrm{MFS}(T) = \log_{10}\mathrm{FS}(T) + \delta\log_{10}\hat{\mathrm{FS}}(T), \qquad (5.2)$$

where $\delta\log_{10}\hat{\mathrm{FS}}(T)$ is the estimated "correction" due to a difference in earthquake magnitude from 6.3 to 6.5, to modification of alluvial depth at the site from h km to h = 2 km, and due to the modification of component direction v (0 for horizontal, or 1 for vertical) to v = 0. From (5.1), this is estimated to be

$$\begin{aligned}\delta\log_{10}\hat{\mathrm{FS}}(T) = {} & 6.5 + \mathcal{A}tt(\Delta_1,6.5,T) + b_1(T)6.5 + b_2(T)2 \\ & + b_4(T)\Delta_1/100 + b_6(T)6.5^2 \\ & - (6.3 + \mathcal{A}tt(\Delta,6.3,T) + b_1(T)6.3 + b_2(T)h \\ & + b_3(T)v + b_4(T)\Delta/100 + b_6(T)6.3^2), \qquad (5.3)\end{aligned}$$

where Δ is the "representative" distance at the site due to the earthquake 6.3, and Δ_1 is the modified representative distance at the same site due to the earthquake of modified magnitude 6.5.

The modified Fourier Spectrum Amplitudes, MFS(T), at 91 periods from 0.04 sec to 15 sec for 1314 components are estimated in this way and stored on a disk file ready for the next step.

Step 3: Since there are frequent fluctuations of Fourier Amplitudes from one period to the next for each of the 1314 components in both the original and in modified database, the period range from 0.04 sec to 15 sec is first divided into 6 bands of approximately equal widths along the logarithmic period scale, with the period ranges given by:

BAND#	Central Period, T (sec)	Period Range (sec)
1	.06	.04 - .10
2	.16	.10 - .24
3	.4	.24 - .65
4	.95	.65 - 1.4
5	2.0	1.4 - 3.2
6	5.0	3.2 - 8.0

The modified Fourier Spectrum Amplitudes, MSF(T), are then divided into 6 groups corresponding to the above 6 period bands. Using the regression coefficients available from Step 1, the data of each period in each group are modified to correspond to the central period of the group. Thus if the amplitude MFS(T) is in the i^{th} group with central period T_i, it is modified to $MFS_i(T)$ corresponding to period T_i by the formula:

$$\log_{10}\hat{MFS}_i(T) = \log_{10}\hat{MFS}(T) + \delta\log_{10}\hat{MFS}_i(T), \qquad (5.4)$$

where $\delta\log_{10}\hat{MFS}_i(T)$ is the estimated "correction" from period T to the central period T_i. It is given by

$$\delta\log_{10}\hat{MFS}_i(T) = \log_{10}\hat{MFS}(T_i) - \log_{10}\hat{MFS}(T) \quad , \qquad (5.5)$$

where $\log_{10}\hat{MFS}(T_i)$ and $\log_{10}\hat{MFS}(T)$ are respectively the estimated logarithms of Fourier Spectrum Amplitudes at periods T_i and T from equation (5.1) at the site with modified magnitude M, h = 2 km and v = 0 (Step 2). The averages of all the resulting amplitudes, $\log_{10}\hat{MFS}_i(T)$, in each period band are then computed. These 6 average modified amplitudes of the 6 bands of each of the 1314 components will be used in the preliminary estimates of the Attenuation Function, $\mathcal{A}tt(\Delta,M,T)$, for each of the four models I, II, III and IV.

For each of the 6 bands, the average Fourier Amplitudes of the 1314 components are least square fitted with the equation:

$$\log_{10}FS = C_0\log_{10}\Delta + C_1 + C_2M + C_3M^2 \qquad (5.6)$$

where M is the magnitude of the earthquake, $\Delta(R,H,S)$ the "representative" distance, R the epicentral distance, H the focal depth and S the "size" of fault, all in km. Note that at each period band, S = S(M) is a linear function of magnitude (4.3) selected as

$$\frac{S-0.2}{M-3} = \frac{S_{6.5}-.2}{3.5} \quad , \text{ or}$$

$$S = 0.2 + \frac{(M-3)}{3.5}(S_{6.5}-.2) \qquad (5.7)$$

The parameter $S_{6.5}$ is still an unknown in each of the 6 period bands. $S_{6.5}$ is interpreted as a "size" of the fault of magnitude 6.5 that if being "felt" at the particular band. Allowing it to range from 1 km to 50 km in (5.7) and substituting the resulting values of S from (5.7) into (5.6), the value of $S_{6.5}$ that gives the best fit of (5.6) can thus be determined. This is repeated for each of the period bands and the values of $S_{6.5}$ and C_o in (5.6) at each band are recorded.

The new frequency dependent attenuation function to be used will be the term corresponding to $C_o \log_{10}\Delta$ in (5.6):

$$\mathcal{A}tt(\Delta,M,T) = \mathcal{A}_o(T)\log_{10}\Delta \qquad (5.8)$$

$\mathcal{A}_o(T)$ will be a parabola to be fitted to the 6 values of C_o of (5.6) determined for the 6 bands. The fault size S = S(T,M) is given by (5.7), with $S_{6.5} = S_{6.5}(T)$ a linear function of T that is fitted to the 6 values of $S_{6.5}$ determined for the 6 bands.

The selection of the new attenuation function is now completed. This new attenuation function can be refined by an iteration of the entire procedure, i.e., by repetition of all previous steps. Steps 2, 3, and 4 above can be repeated using the new attenuation function and the updated attenuation function can be compared with the previous one until there is satisfactory "convergence" of the term $\mathcal{A}_o(T) \log_{10}\Delta$.

During the subsequent iterations, it has been found that the linear term in Δ in (5.1), namely. $b_4(T)$ /100, has the coefficient $b_4(T)$ which is insignificant for most of the periods. Subsequently, this term has been deleted from the regression analysis and the empirical scaling equation, (5.1), thus becomes:

$$\log_{10}FS(T) = M + \mathcal{A}tt(\Delta,M,T) + b_1(T)M + b_2(T)h + b_3(T)v + b_5(T) + b_6(T)M^2 \quad (5.9)$$

6. The Attenuation Function at Large Distances

The procedures described in the previous section for the four proposed models will determine the attenuation of strong-motion amplitudes for the distances within 100 to 150 km from the source of an earthquake. At distances exceeding this range, we expect the strong-motion data to consist primarily of surface waves and that the attenuation of recorded strong-motion amplitudes would then be slower than for the sites closer to the source. At these and larger distances the recorded strong-motion amplitudes become small and consist of longer periods, so that, especially for smaller magnitude earthquakes, strong-motion accelerographs may not trigger. Consequently at these and larger distances the lack of recorded strong-motion data at present does not allow reliable estimates of the attenuation functions. To take this into account at large distances, (5.8) is combined with (1.5) so that the attenuation function will have the empirically determined slope of -1/200 (equation (1.5)). The new attenuation function is thus modified to be of the form

$$\mathcal{A}tt(\Delta,M,T) = \begin{cases} \mathcal{A}_0(T)\log_{10}\Delta & R \le R_0 \\ \mathcal{A}_0(T)\log_{10}\Delta_0 - (R-R_0)/200 & R > R_0 \end{cases}, \quad (6.1)$$

where Δ is the representative distance as defined in any of the four models above, and Δ_0 is the corresponding representative distance at the transition distance R_0. The attenuation function is as that given

by (5.8) at distances R less than R_0. For distances $R > R_0$, it is a linear function with slope -1/200 as in (1.5). The slope of the attenuation function for $R \leq R_0$ depends on the epicentral distance, R, the focal depth, H, the source dimension, S, and on the period of the wave, T. Taking the cutoff distance R_0 to be 75 km as in the case of Richter's Attenuation Function would be inappropriate, as this would result in discontinuity of the slope of the function at $R = R_0$.

Therefore, R_0 is determined from the requirement that the slope of the function (5.8) equals -1/200. It is determined for each of the four attenuation models as follows:

(a) Model I, $\Delta = (R^2 + H^2 + S^2)^{\frac{1}{2}}$

The slope of the attenuation function is given by (from (5.8)):

$$\frac{d}{dR}(\mathcal{A}tt(\Delta,M,T)) = \frac{d}{dR}(\mathcal{A}_0(T)\log_{10}(R^2 + H^2 + S^2)^{\frac{1}{2}})$$

$$= \frac{\mathcal{A}_0(T)R}{(R^2 + H^2 + S^2)\ell n10}, \qquad (6.2)$$

which when equated to the constant slope of -1/200, gives

$$R^2 + \frac{200\mathcal{A}_0(T)}{\ell n10} R + H^2 + S^2 = 0, \qquad (6.3)$$

a quadratic equation in R. The solution, R_0, the transition distance, is the larger of the 2 roots, is

$$R_0 = \frac{1}{2}\left(\frac{-200\mathcal{A}_0(T)}{\ell n10} + \sqrt{\frac{4 \times 10^4 \times \mathcal{A}_0^2(T)}{(\ell n10)^2} - 4(H^2 + S^2)}\right), \qquad (6.4)$$

and is a function of H, S (hence a function of M) and $\mathcal{A}_0(T)$. At long periods and larger magnitudes, M, when the source S is large and the attenuation term $\mathcal{A}_0(T)$ small, the square-root term (discriminant) in (6.4) becomes negative and hence R_0 becomes complex. In such cases, for simplicity only, the first term of (6.4) has been taken as an estimate of the transition distance, i.e. $R_0 = -100\mathcal{A}_0(T)/\ell n10$.

(b) Model II, $\Delta = (R^2 + H^2 + S^2)^{\frac{1}{2}}$

Equating the slope of the function in (5.8) as in Model I would lead to the equation

$$R^2 + \frac{200\mathcal{A}_0(T)}{\ell n10} R + H^2 + \hat{S}^2 = 0 \qquad (6.5)$$

Since from (4.6), $\hat{S} = S(1.-\exp(\ell n(.1)R/R)$, $\hat{S}$ is now also a function of R, and thus (6.5) becomes a transcendental equation in R. However, the transition distance R_0 is usually at a distance much further out than the size of the fault S, i.e. $R_0 >> S$, so that a first approximation of R_0 can be obtained by taking $\hat{S} = S$, so that equation (6.5) reduces to (6.3), and the solution R_0 is given by (6.4). With this first approximation, $\hat{S}$ can be calculated from

$$\hat{S} = S(1-\exp(\ell n(.1)R_0(S)) \qquad (6.6)$$

subsituting R_0 for R. With this value of $\hat{S}$, (6.5) can then be solved as a quadriatic equation to get R_0. By substituting this updated value of R_0 back to $\hat{S}$ and iterating a few times will converge to the solution R_0. The same comments for R_0 in Model I apply here.

(c) Model III, $\Delta = S\left(\ell n \frac{R^2 + H^2 + S^2}{R^2 + H^2 + S_0^2}\right)^{-\frac{1}{2}}$

The slope of the attenuation function (5.8) can again be obtained by differentiating $\mathcal{A}_0(T)\ell n\Delta$, but this will result in a complicated transcendental equation for R. Again, since the transition distance R_0 is much further out than the fault size, i.e. $R_0 >> S$, an asymptotic solution is taken. For the case when $R^2 + H^2 >> S$, an asymptotic expansion of Δ (equation (4.11) is given by

$$\Delta \sim ((R^2 + H^2)/(1-S_0^2/S^2)^{\frac{1}{2}} . \qquad (6.7)$$

Using (6.7), the slope of the attenuation function is then

$$\frac{d}{dR}(\mathcal{A}tt(\Delta,M,T)) = \frac{d}{dR}(\mathcal{A}_0(T)\log_{10}\Delta)$$

$$\sim \frac{\mathcal{A}_0(T)(1-S_0^2/S^2)R}{(R^2 + H^2)\ell n10} , \qquad (6.8)$$

which when equated to the constant slope of -1/200, gives

$$R^2 + \frac{200\mathcal{A}_0(T)(1-S_0^2)}{\ell n10} R + H^2 = 0 \qquad (6.9)$$

another quadriatic equation in R. The solution, R_0, is given by

$$R_0 = \frac{1}{2}\left(\frac{-200\mathcal{A}_0(T)(1-S_0^2/S^2)}{\ell n10} + \sqrt{\frac{200\mathcal{A}_0(T)(1-S_0^2/S^2)}{\ell n10} - 4H^2}\right) \qquad (6.10)$$

similar to the expressions for Models I and II (equation (6.4)).

(d) Model IV, $\Delta = \hat{S}\left(\ell n \frac{R^2 + H^2 + S^2}{R^2 + H^2 + S_o^2}\right)^{-\frac{1}{2}}$

Substituting $\hat{S}$ for S in (6.7) gives the asymptotic expansion as

$$\Delta \sim ((R^2 + H^2)/(1-S_o^2/S^2))^{\frac{1}{2}} \tag{6.11}$$

which will result, as above, in the following quadriatic equation:

$$R^2 + \frac{200\mathcal{A}_o(T)(1-S_o^2/S^2)}{\ell n 10} R + H^2 = 0. \tag{6.12}$$

Since from (4.12),

$$\hat{S} = \min\{S,(R^2 + H^2)^{\frac{1}{2}}\} \tag{6.13}$$

(6.12) is again a transcendental equation in R. Again, the assumption, $S^2 << R^2 + H^2$, can be applied here to give $\hat{S} = S$, so that (6.12) can be solved as in (6.9)

7. Results I: Model I, $\Delta = (R^2 + H^2 + S^2)^{\frac{1}{2}}$

The "convergence" of the attenuation function $\mathcal{A}_o(T)\log_{10}\Delta$ was found to be very satisfactory just after a few iterations of the above procedure. Figures 7.1 through 7.6 show plots of the average Fourier Amplitudes from the modified database for magnitudes in the ranges from 3.5 to 7.5 in each of the six period bands. Band 1 corresponds to the low period high frequency end, and with increasing periods, Band 6 corresponds to the long period, low frequency end. The top dashed line in each figure, shown with arbitrary amplitude scale and for easy comparison of the overall attenuation function shapes, is the Richter's attenuation function, while the other dashed lines in each band are the

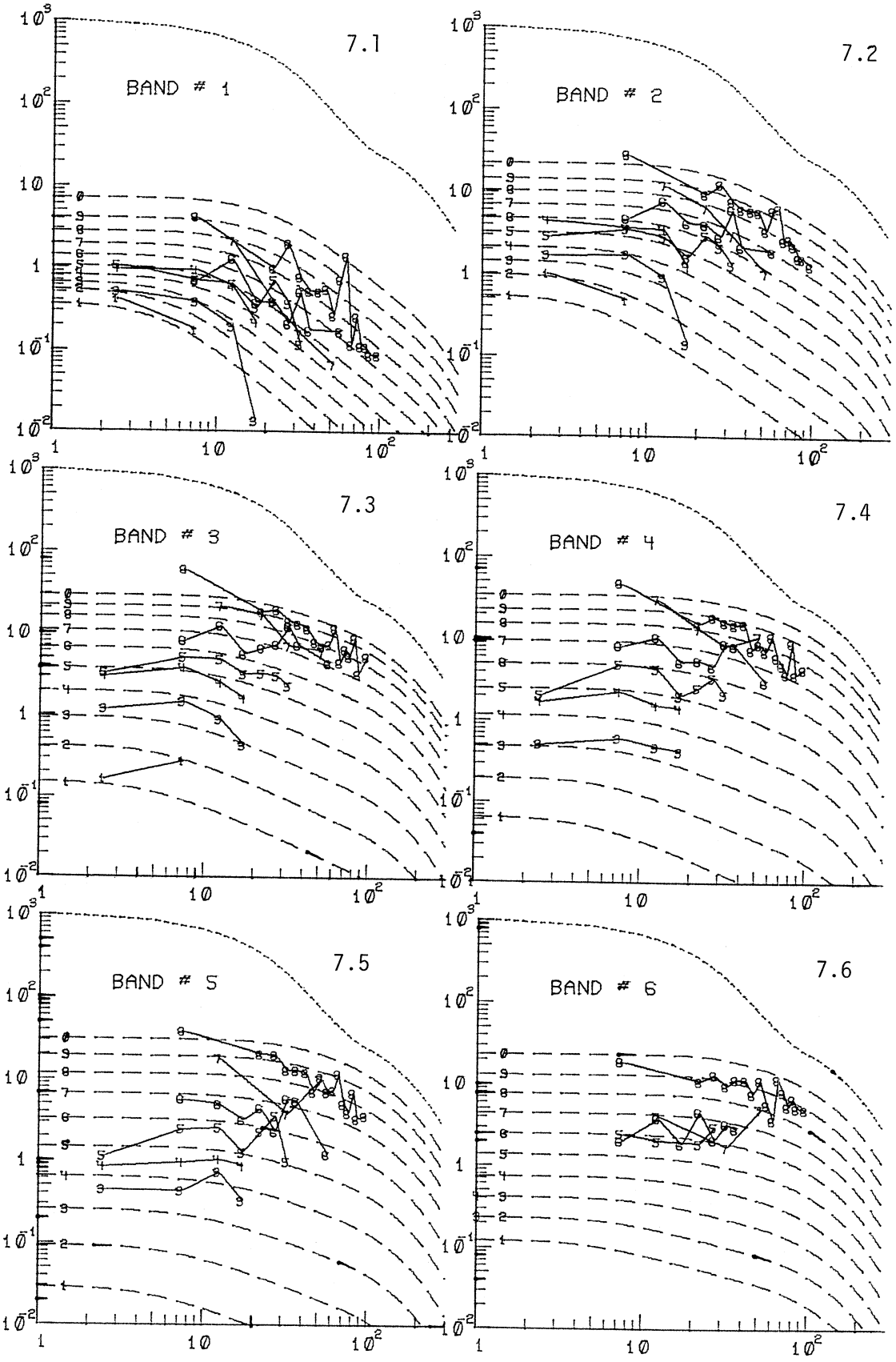

Figures 7.1-7.6 - Average modified FS amplitudes (full irregular lines) for M = 3.5(1), 4.5(2), 5.0(3), 5.5(4).... 7.0(8) and 7.5(9) at 6 period bands. Dashed lines represent the corresponding amplitude trends predicted by the regression Model I. Top dotted line illustrates the shape of $\log_{10} A_o(R)$ attenuation law.

corresponding estimated amplitudes using (5.6), with the attenuation function given by (6.1).

The estimated final values of $S_{6.5}$ and C_0 used on (5.6) for the 6 bands are given in Table 7-1. The straight line from least-squares fit of the values of $S_{6.5}$ is shown in Figure 7.7 and the parabolic fit to C_0 in Figure 7.8. Only the points in the first five bands have been used in the regression analysis in both cases, as it is found that the sixth band in the long period end is often contaminated with long period noise.

Note that for the low period, high frequency band (Band #1), from 10 km on, the Fourier amplitudes attenuate very rapidly to almost 150 km before the attenuation levels off to the slope of -1/200. This is true at all magnitude ranges. The transition distances, R_0 for the transition at this low period, high frequency end are as high as 150 km for most magnitude ranges. As the period range increases from Band #2 onwards through Band #6, the above described amplitude attenuation slopes of -1/200 are at decreasing cutoff distances from R_0 = 150 km at the low period end to as low as 40 km at the long period end (Band #6). This is why as the Band number increases, the estimated attenuation of the Fourier amplitudes is seen to agree in slope with the Richter's attenuation curve at gradually decreasing distances. Figure 7.9 is a plot of these transition distances, R_0, versus periods, T, in (6.4) for magnitudes M = 4,5,6 and 7. Note that for magnitude M = 7, the cutoff distance, R_0, levels to a constant at a period not much after 1 sec. This is because the discriminant in (6.4) is negative at those periods and we choose, arbitrarily, only the first term of (6.4) to estimate R_0.

TABLE 7-1

Band #	Range (Sec.)	$S_{6.5}$	C_o
1	.04-.10	18	-1.86708
2	.10-.24	25	-1.52468
3	.24-.65	25	-1.03379
4	.65-1.4	30	-.908991
5	1.4-3.2	32	-.92390
6	3.2-8.0	34	-.871122

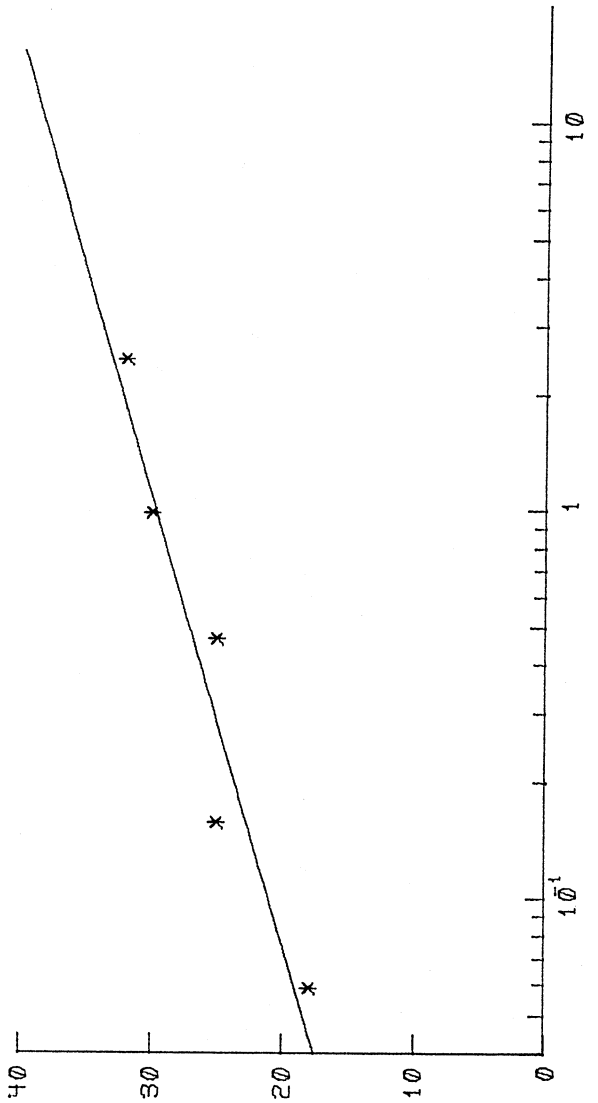

Figure 7.7 - Least Square (Straight Line) Fit of $S_{6.5}$: Model I

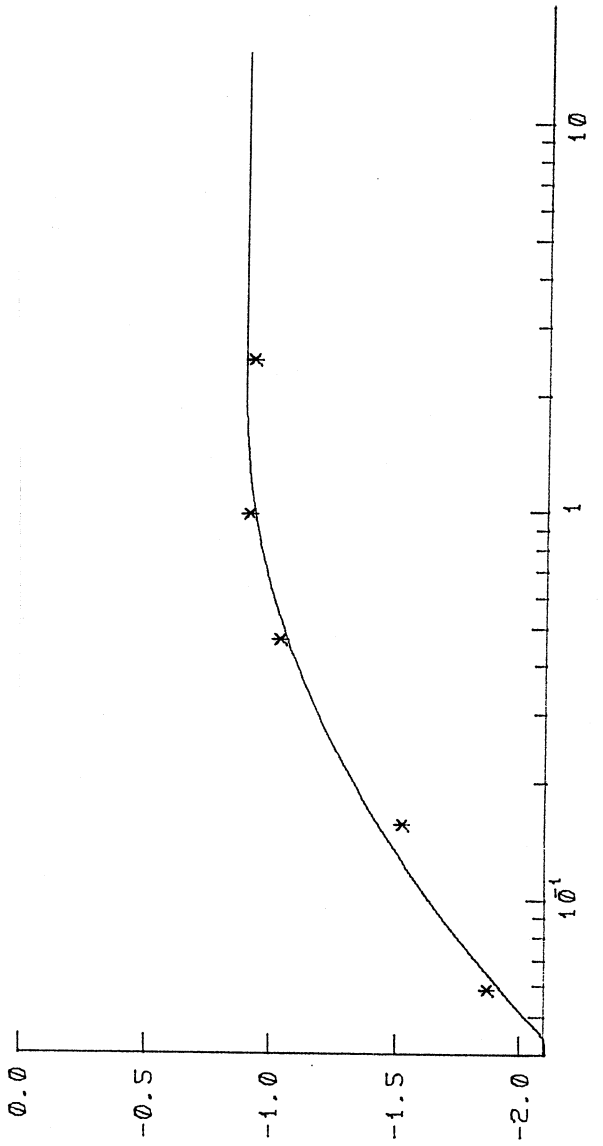

Figure 7.8 - Least Square (Parabolic) Fit of C_o: Model I

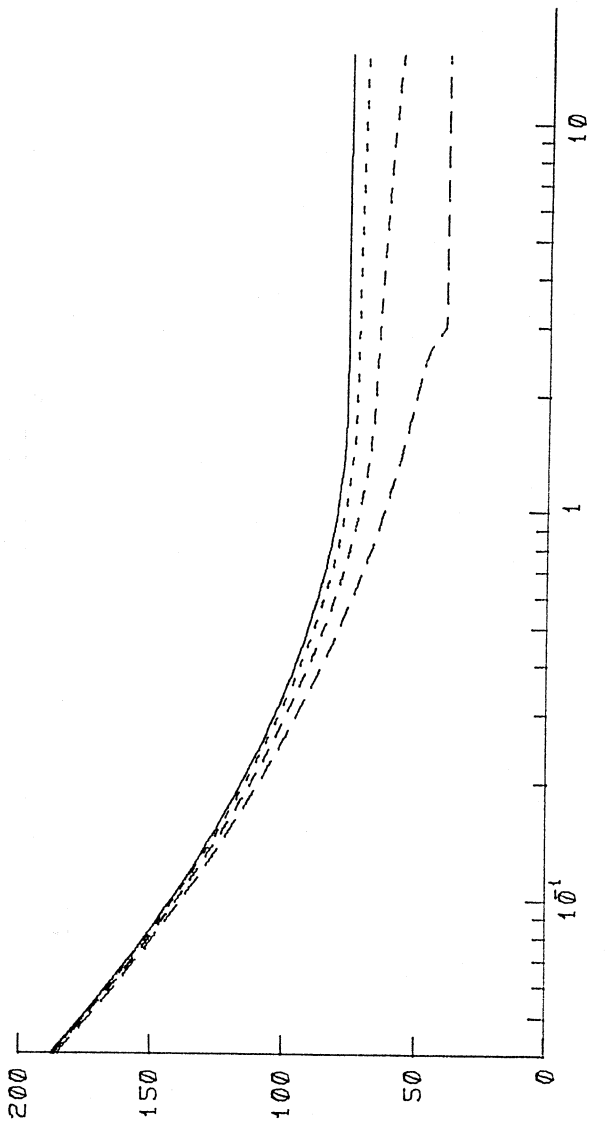

Figure 7.9 - Transition Distances R_o for M = 4, 5, 6, 7: Model I

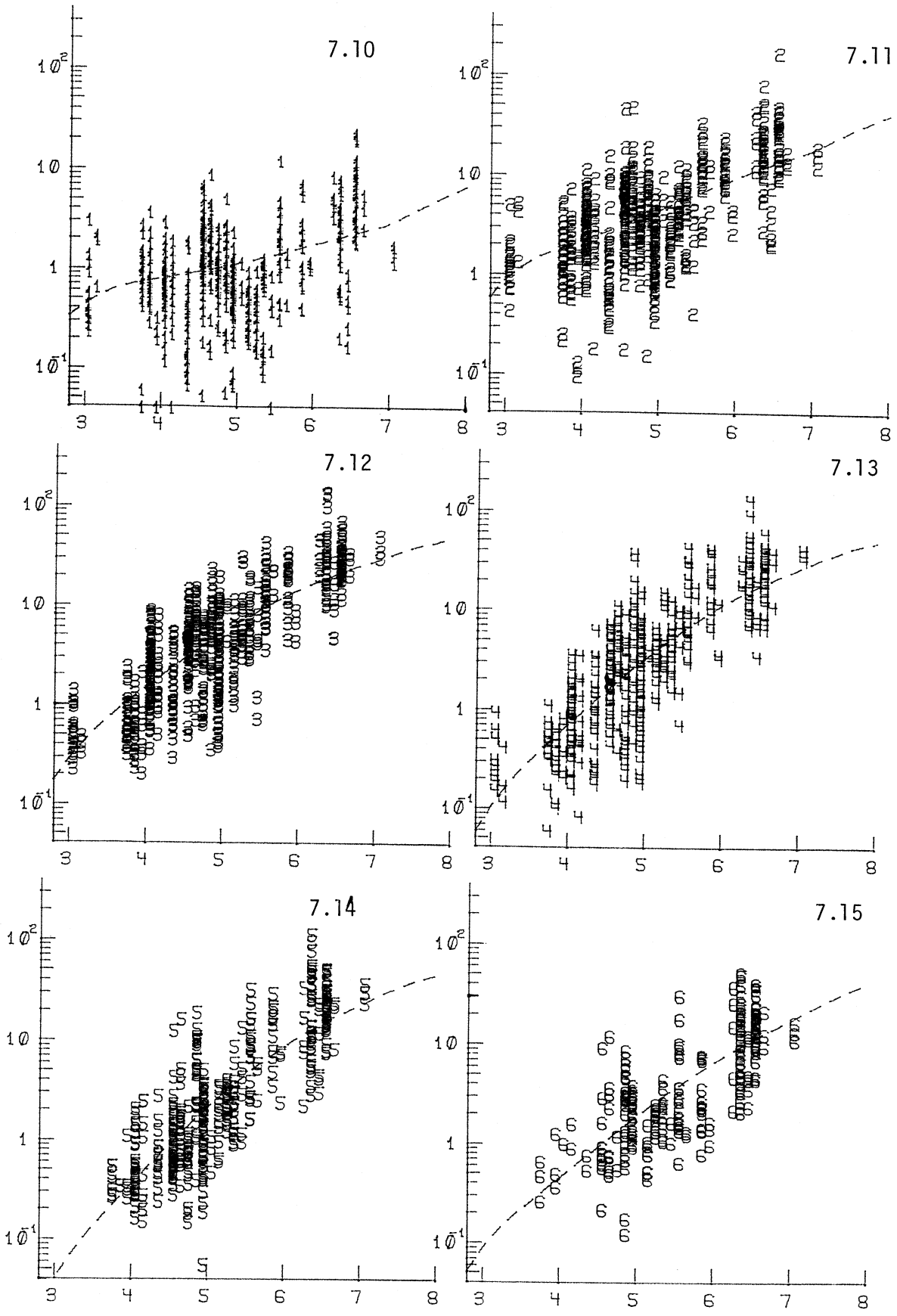

Figures 7.10-7.15 - Estimated (Dashed Lines) and Normalized FS Amplitudes versus M at R = 0 km: Model I. Arabic numerals indicate the band number.

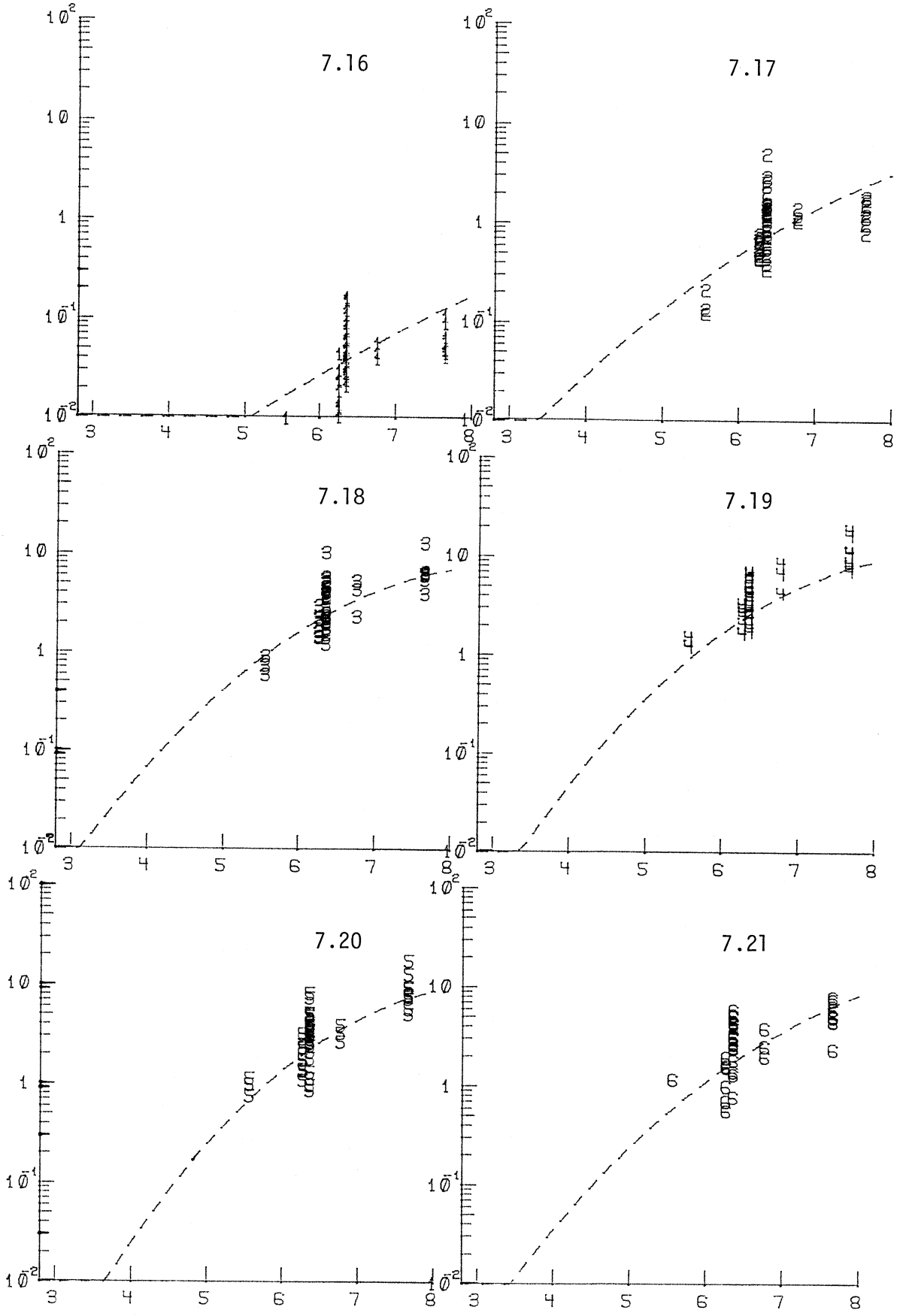

Figures 7.16-7.21 - Estimated (Dashed Lines) and Normalized FS Amplitudes versus M at R = 150 km: Model I. Arabic numerals indicate the band number.

To test the performance of the above attenuation function, a normalized database of Fourier amplitudes has been prepared from the original 1314 acceleration components. Two groups of data have been first selected from the database. The first group consisted of data recorded at epicentral distances $R \leq 30$ km and the second group consisted of data at epicentral distances in the range $100 \leq R \leq 200$ km. The database of this new normalized Fourier spectral amplitudes, $NFS_1(T)$, from the first group is to consist of data with the original magnitudes, M, but with alluvial depth h normalized to h = 2 km, component parameter v to v = 0 (horizontal), and is to correspond to the recordings at zero distance, R = 0 km. Similarly, the database normalized in the second group is to correspond to the data recorded at an epicentral distance of R = 150 km with h = 2 km and v = 0. The 6 bands of noramlized Fourier amplitudes of the first group (at R = 0) are plotted versus magnitudes in the range from M = 3 to M = 8 in Figures 7.10 through 7.15. The dashed line in each plot corresponds to the estimated Fourier amplitudes versus magnitude at R = 0 using equation (5.6) with the estimated attenuation term $C_0 \log_{10}\Delta$ calculated as above. The 6 bands of normalized Fourier amplitudes of the second group (at R = 150 km) are plotted in Figures 7.16 through 7.21, together with the estimated amplitudes as dashed lines.

8. Results: Model II, $\Delta = (R^2 + H^2 + S^2)^{\frac{1}{2}}$

With the modified definition of the fault size (equation (4.6)) in Model II, the iteration steps described in Section 5 have been repeated to estimate the new attenuation function $\mathcal{A}_0(T)\log_{10}\Delta$. Agreement was

again found to be very satisfactory just after two or more iterations of the procedure described in Section 5.

Figures 8.1 through 8.6 are plots of the average Fourier Amplitudes from the modified database using the new definition of Δ and for magnitudes in the range from 3.5 to 7.5 in each of the period bands. Table 8-1 gives the estimated values of $S_{6.5}$ and C_0 used in (5.6).

Figure 8.7 shows the straight line from the least squares fit of the first five values of $S_{6.5}$, and Figure 8.8 the parabolic fit for C_0. As in the previous section, only five points in the first five bands are used in both cases. The average value os $S_{6.5}$ is now about 17.5 as compared to 27.5 in the previous section. The shape of the parabola is similar to that from the previous section.

Figure 8.9 is a plot of the transition distances R_0, versus periods, T, in (6.4) for magnitudes M = 4,5,6 and 7, using the new definition of fault size, $\hat{S}$ and the new estimated values of $\mathcal{A}_0(T)$. Similar to the previous case (Fig. 7.7), the transition distances R_0 start from as high as 150 km at short periods and decrease to about 60 km at long periods.

As in the previous section, overall performance of the new attenuation function is tested as follows. A normalized set of Fourier amplitudes has been prepared as in the previous section. This resulted in 2 groups of normalized data, one at epicentral distance of R = 0 km and the other at R = 150 km. Both groups of data were normalized using the new attenuation function. The 6 bands of normalized data of the first group (at R = 0 km) have been plotted versus magnitude in Figures 8.10 through 8.15. When compared with the corresponding normalized data in the previous section (Fig. 7.10 through 7.15), the

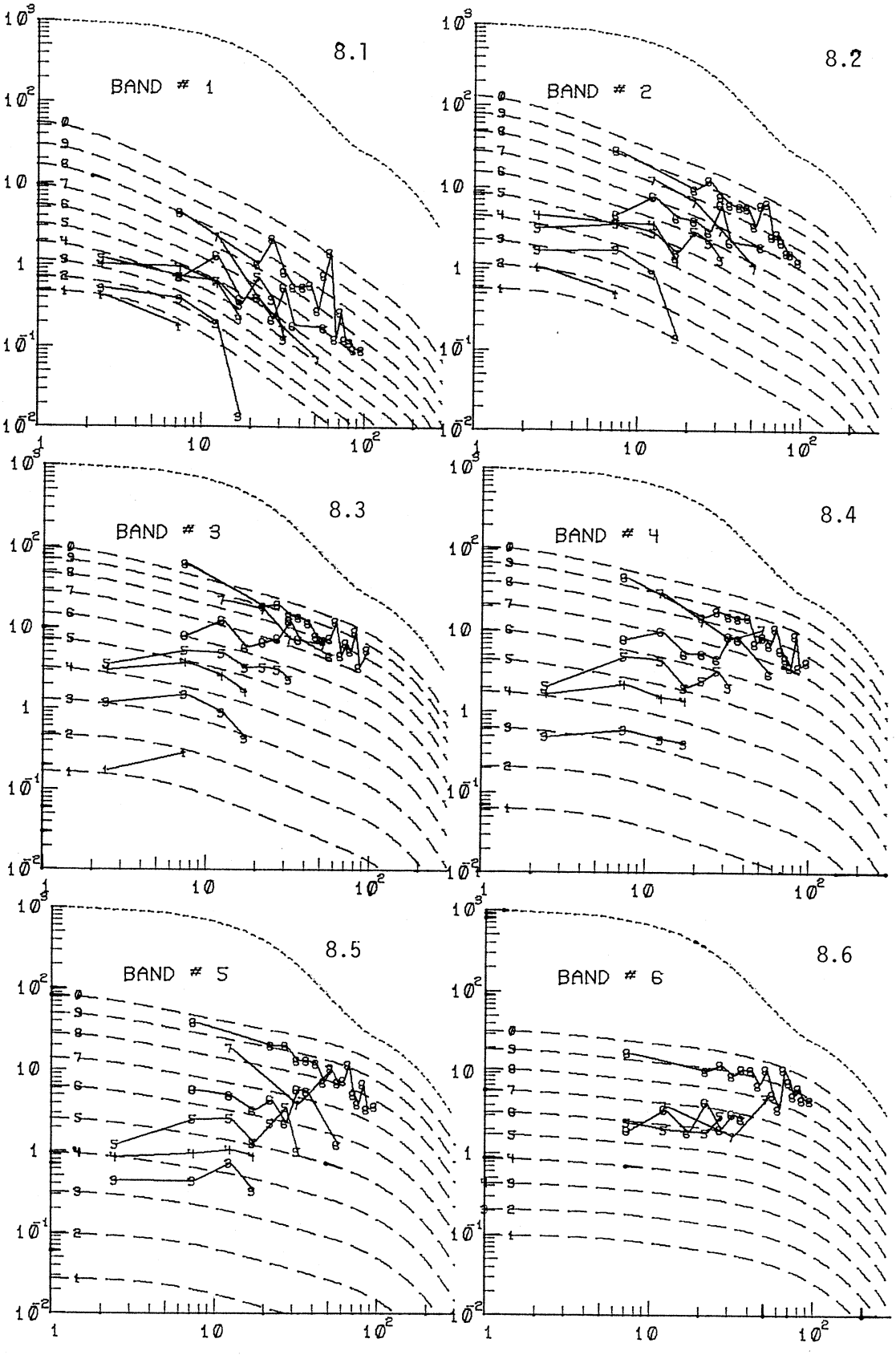

Figures 8.1-8.6 - Average modified FS amplitudes (full irregular lines) for M = 3.5(1), 4.5(2), 5.0(3), 5.5(4)....7.0(8) and 7.5(9) at 6 period bands. Dashed lines represent the corresponding amplitude trends predicted by the regression Model II. Top dotted line illustrates the shape of $\log_{10} A_o(R)$ attenuation law.

TABLE 8-1

Band #	Range (Sec.)	$S_{6.5}$	C_o
1	.04-.10	16	-1.75888
2	.10-.24	21	-1.35071
3	.24-.65	18	-.891877
4	.65-1.4	18	-.719342
5	1.4-3.2	20	-.725126
6	3.2-8.0	23	-.640947

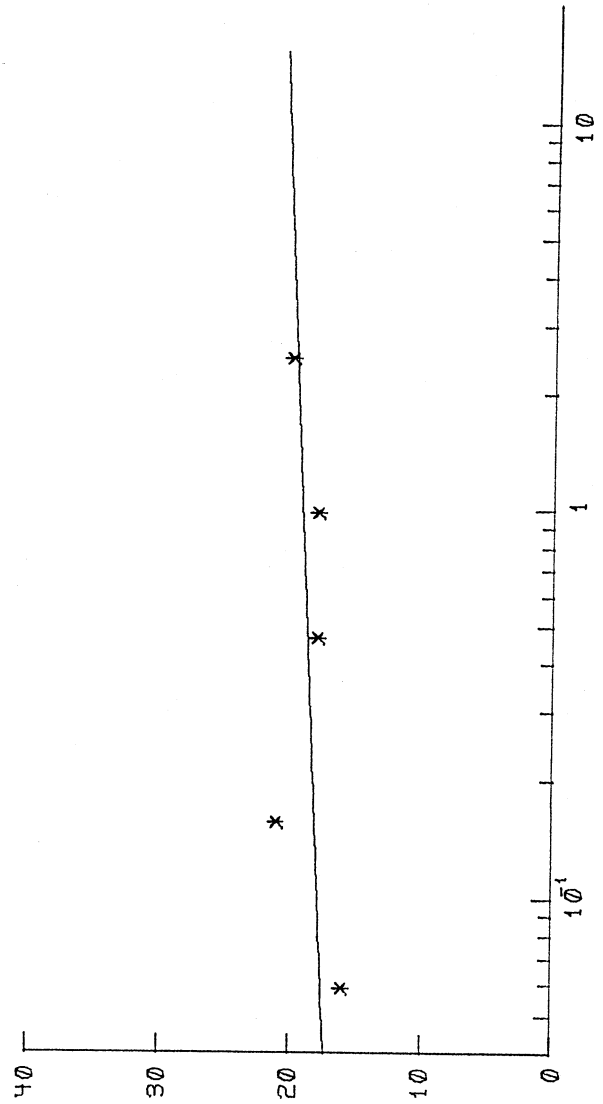

Figure 8.7 - Least Square (Straight Line) Fit of $S_{6.5}$: Model II

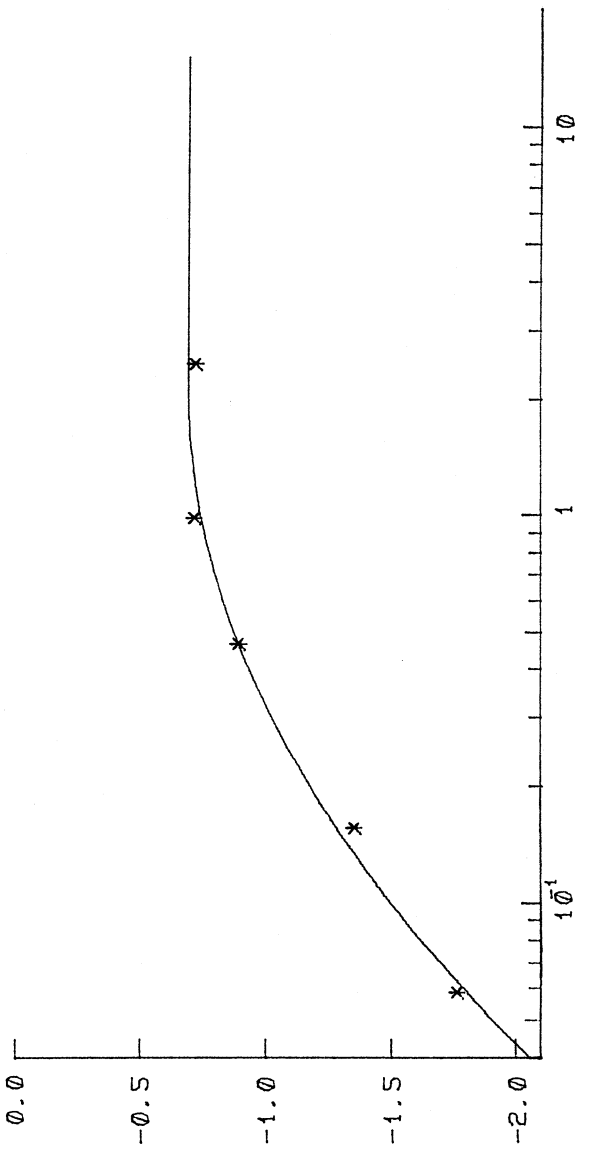

Figure 8.8 - Least Square (Parabolic) Fit of C_o: Model II

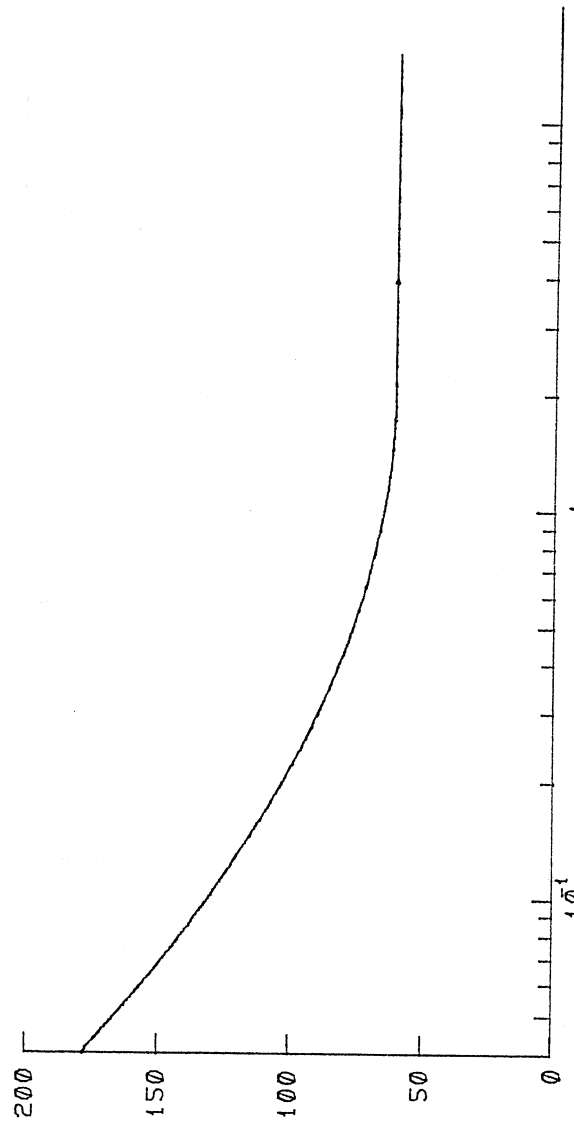

Figure 8.9 - Transition Distances R_o for M = 4, 5, 6, 7: Model II

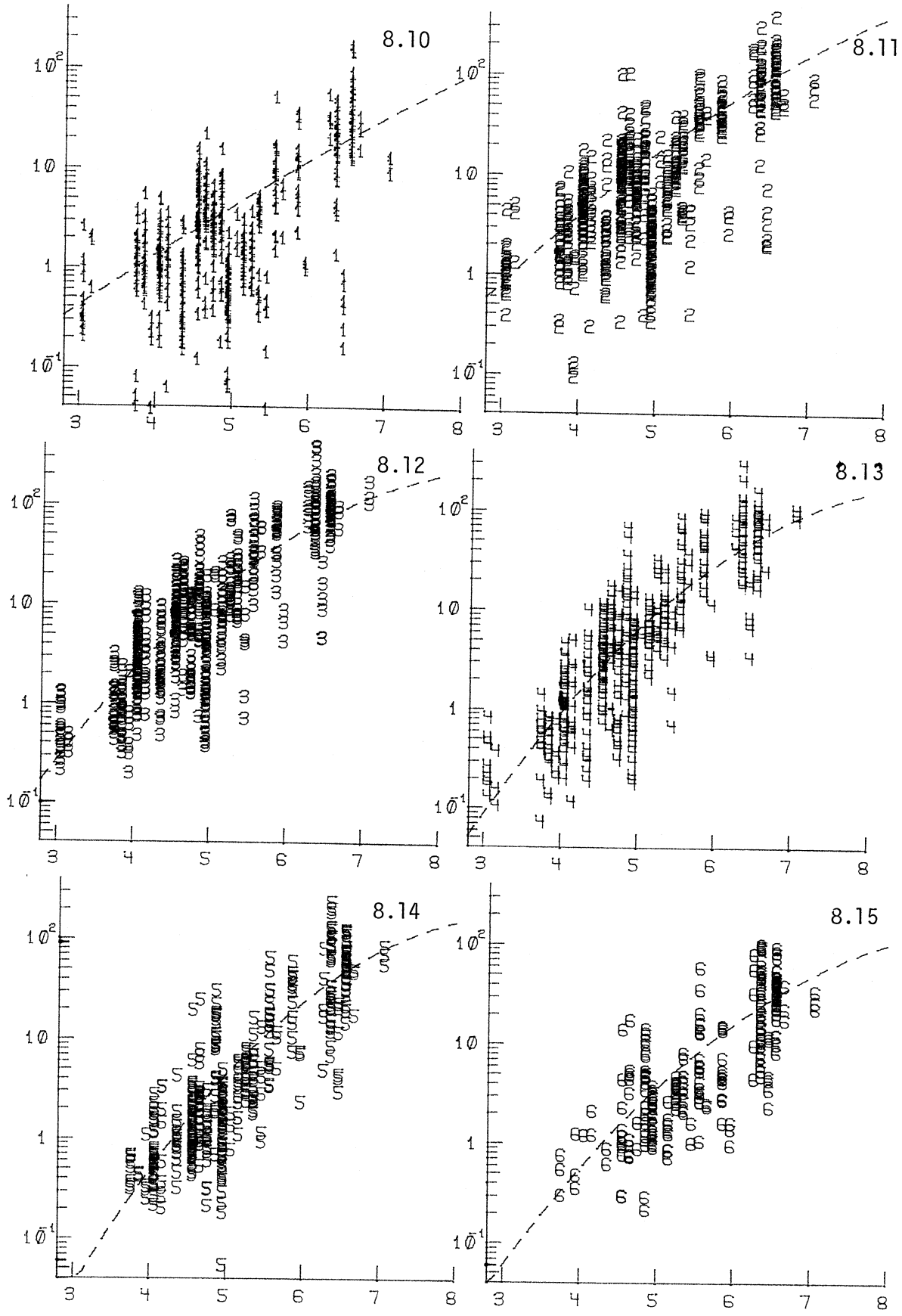

Figures 8.10-8.15 - Estimated (Dashed Lines) and Normalized FS Amplitudes versus M at R = 0 km: Model II. Arabic numerals indicate the band number.

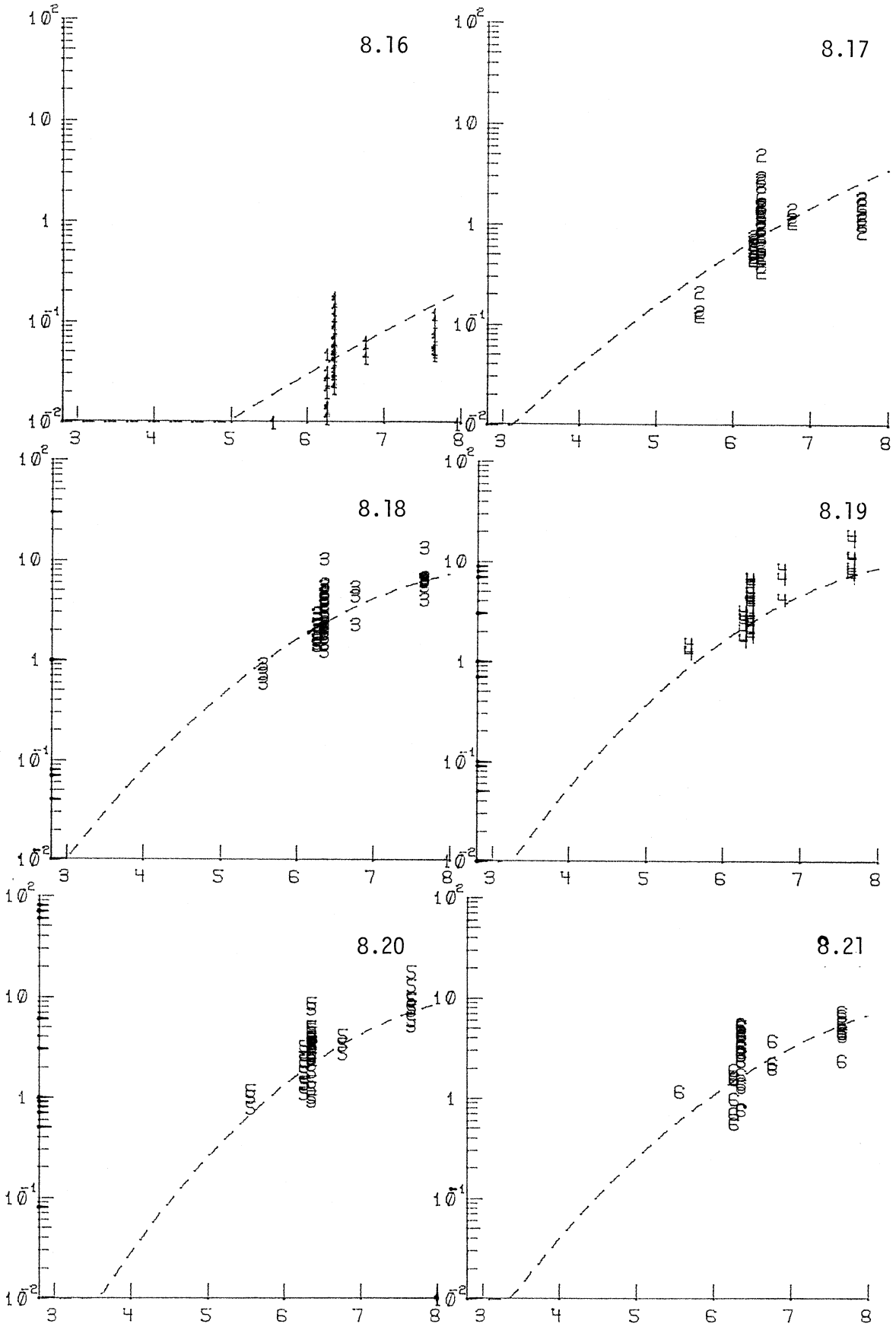

Figures 8.16-8.21 - Estimated (Dashed Lines) and Normalized FS Amplitudes versus M at R = 150 km: Model II. Arabic numerals indicate the band number.

amplitudes of each point are higher using the new attenuation function in all period bands. The same holds for the estimated amplitudes (dashed line) using equation (5.6). Similarly, the 6 bands of normalized Fourier amplitudes of the second group (at R = 150 km) are plotted in Figures 8.16 through 8.21 together with the estimated amplitudes as dashed lines. When compared with the previous section (Fig. 7.16 through 7.21), the amplitudes are very similar, meaning that the attenuation functions are practically identical at large distances.

9. Results: Model III, $\Delta = S\left(\ell n \frac{R^2 + H^2 + S^2}{R^2 + H^2 + S_o^2}\right)^{-\frac{1}{2}}$

With this definition of representative distance Δ in Model III, the iteration steps described in Section 5 have been repeated. One difference between this and the previous two Models, I and II, is the introduction of the new parameter, S_o, in the definition of Δ. Here S_o corresponds to the correlation distance of the subsources at the fault plane. Step 3 of the iteration procedure in Section 5 thus has been modified to include the estimation of S_o. Different sizes of S_o, expressed as the ratio S_o/S, with values equal to .025, .05, .075, .1, .2, .3, .4 and .5, have been used. The analysis shows that the results are not sensitive to these different ratios at all. Thus, using (4.7) the following empirical estimate for S_o was adopted

$$S_o = \min(\lambda/2, S/2) \qquad (9.1)$$

with $\lambda = C_s T$ and assuming C_s = 1 km/sec. Thus the correlation radius is either half of the wavelength of the corresponding period T or half of the fault size, whichever is smaller.

Using this definition of S_0, the "convergence" of the attenuation function $\mathcal{A}_0(T)\log_{10}\Delta$ was again found to be very satisfactory just after a few iterations.

Figures 9.1 through 9.6 show plots of the average Fourier Amplitudes from the modified database using the definition of Δ in Model III and for magnitudes in the range from 3.5 to 7.5 in each of the six period bands. Table 9-1 gives the estimated values of $S_{6.5}$ and C_0 used in (5.6). Figure 9.7 shows the straight line from the least squares fit of the first five values of $S_{6.5}$, and Figure 9.8 the parabolic fit for C_0. Figure 9.9 is a plot of the transition distance R_0, versus periods, T, in (6.10) for Model III, and for magnitudes M = 4,5,6 and 7. As for the previous models, the transition distances R_0 start from as high as 150 km at short periods and decrease to as low as 50 km at long periods.

As in the previous models, the overall performance of the new attenuation function is tested. Again a normalized set of Fourier amplitudes has been prepared, resulting in 2 groups of data, one at epicentral distance of R = 0 km and the other at R = 150 km. The 6 bands of normalized data of the first group (at R = 0 km) have been plotted versus magnitude in Figures 9.10 through 9.15. The estimated amplitudes (dashed line) are calculated and plotted using equation (5.6). Similarly, the data of the second group (R = 150 km) are plotted in Figures 9.16 through 9.21. The two groups of plots show that the Model III attenuation function behaves like that of Model I at short distances, while all three models considered so far are practically identical at large distances.

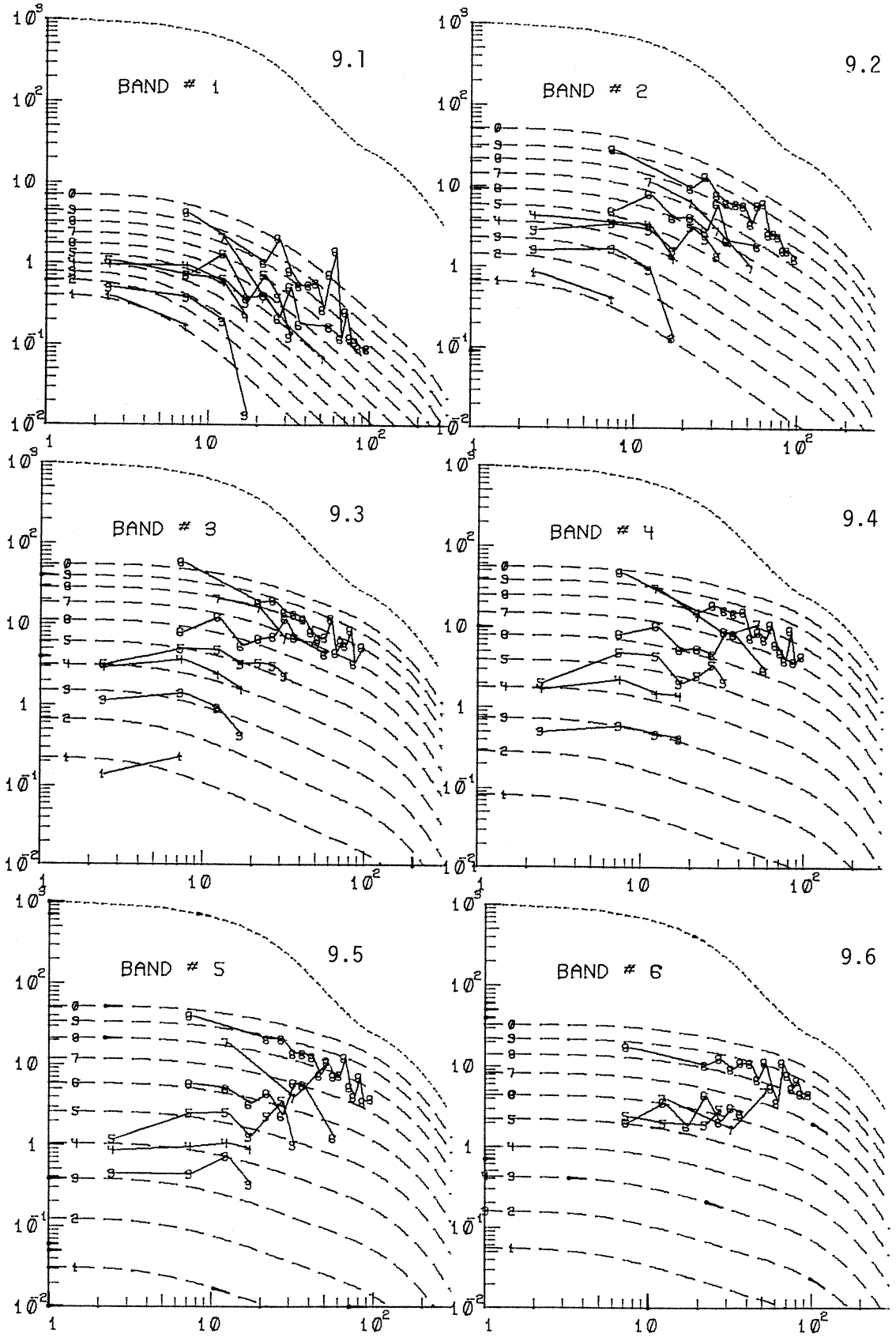

Figures 9.1-9.6 - Average modified FS amplitudes (full irregular lines) for M = 3.5(1), 4.5(2), 5.0(3), 5.5(4)....7.0(8) and 7.5(9) at 6 period bands. Dashed lines represent the corresponding amplitude trends predicted by the regression Model III. Top dotted line illustrates the shape of $\log_{10} A_o(R)$ attenuation law.

TABLE 9-1

Band #	Range (Sec.)	$S_{6.5}$	C_o
1	.04-.10	29	-1.86209
2	.10-.24	30	-1.37171
3	.24-.65	30	-.928757
4	.65-1.4	30	-.750504
5	1.4-3.2	30	-.751518
6	3.2-8.0	30	-.654003

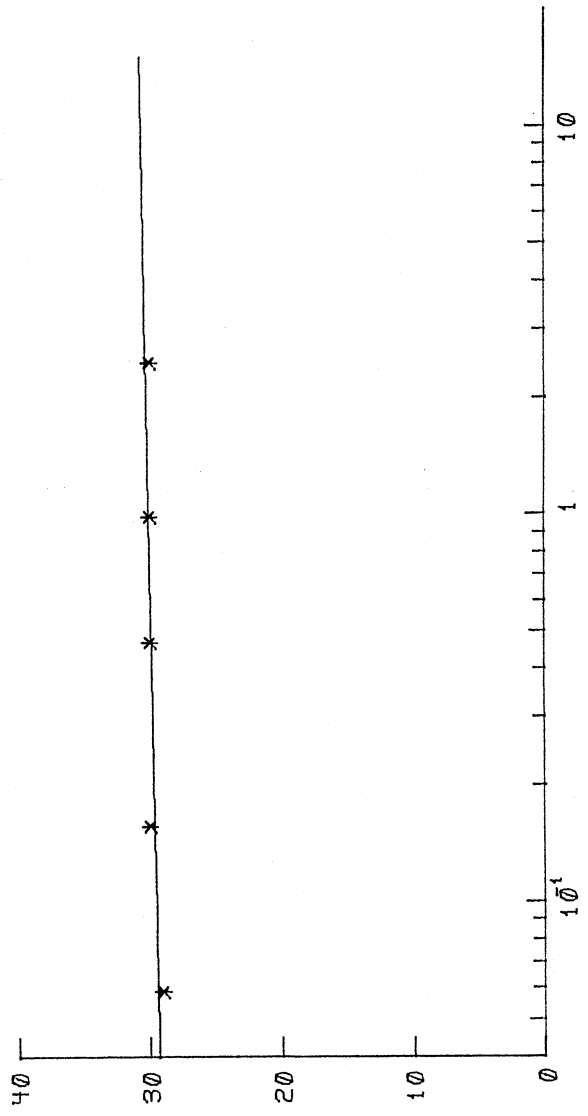

Figure 9.7 - Least Square (Straight Line) Fit of $S_{6.5}$: Model III.

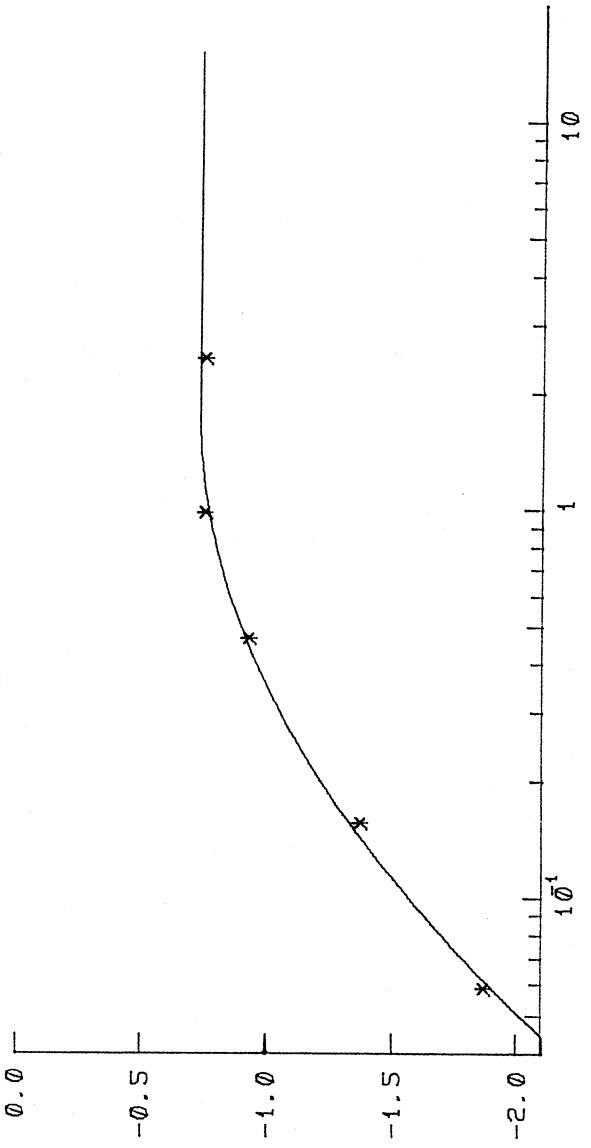

Figure 9.8 - Least Square (Parabolic) Fit of C_o: Model III.

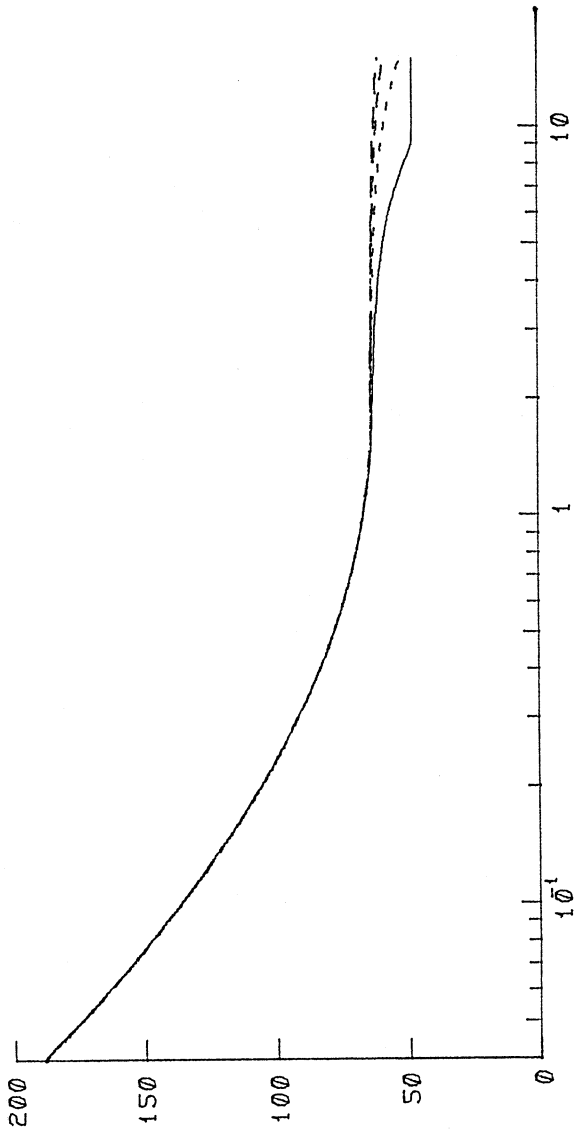

Figure 9.9 - Transition Distances R_0 for M = 4, 5, 6, 7: Model III.

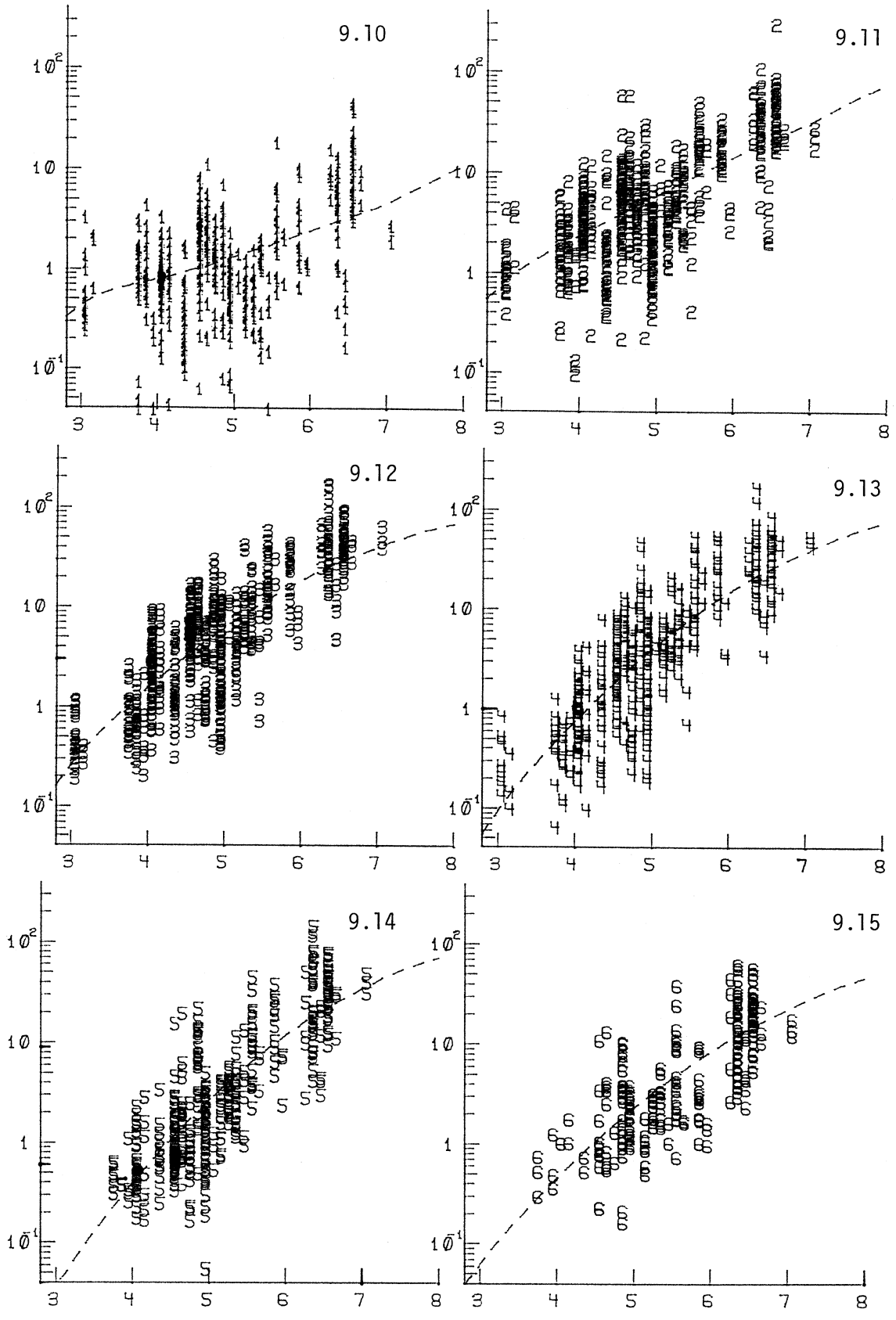

Figures 9.10-9.15 - Estimated (Dashed Lines) and Normalized FS Amplitudes versus M at R = 0 km: Model III. Arabic numerals indicate the band number.

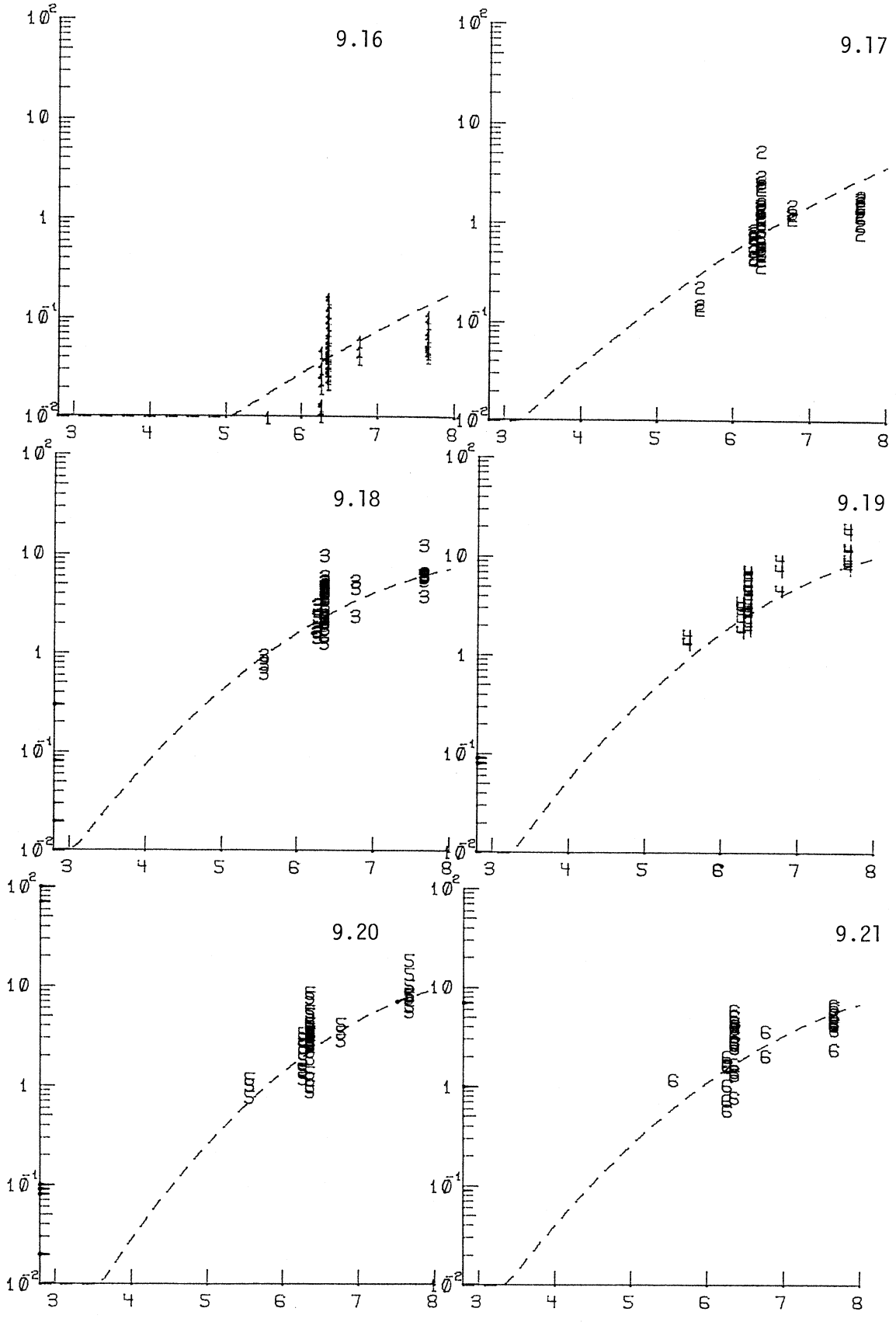

Figures 9.16-9.21 - Estimated (Dashed Lines) and Normalized FS Amplitudes versus M at R = 150 km: Model III. Arabic numerals indicate the band number.

10. Results: Model IV, $\Delta = S\left(\ell n \frac{R^2 + H^2 + \hat{S}^2}{R^2 + H^2 + S_o^2}\right)^{-\frac{1}{2}}$

Repeating the iteration procedures in Section 5 using the representative distance Δ for Model IV, the results are presented in Table 10-1 and in Figures 10.1 through 10.21 as in all previous models. Using the modified definition of fault sizes (equation (4.12)), the estimated amplitudes in 6 bands now attenuate faster than those described by Model III in Figures 9.1 through 9.6. The normalized data of the first group (at R = 0 km) as plotted in Figures 10.10 through 10.15 are now higher in amplitudes than the corresponding data of Model III in Figures 9.10 through 9.15. However, when comparing the normalized data of the second group (at R = 150 km) in Figures 10.16 through 10.21 with those from Model III in Figures 9.16 through 9.21, it is found that those are practically identical, which shows again that the attenuation functions at large distances all behave in the same way.

The results from all four models have now been presented. One additional useful comparison of the four models is to calculate the root-mean-squared values of the residues of the fit at the six bands from all four models:

$$\sigma = \left(\sum \varepsilon_i^2\right)^{\frac{1}{2}} = \left(\sum_i \left(\log_{10} FS_i - \log_{10} \hat{FS}_i\right)^2\right)^{\frac{1}{2}} \qquad (10.1)$$

where $\log\hat{FS}_i$ is the estimated amplitude computed from (5.6). The results for all 4 models at the six bands are plotted in Figure 10.22, which shows that for the four models the R.M.S. values of the residues are not significantly different.

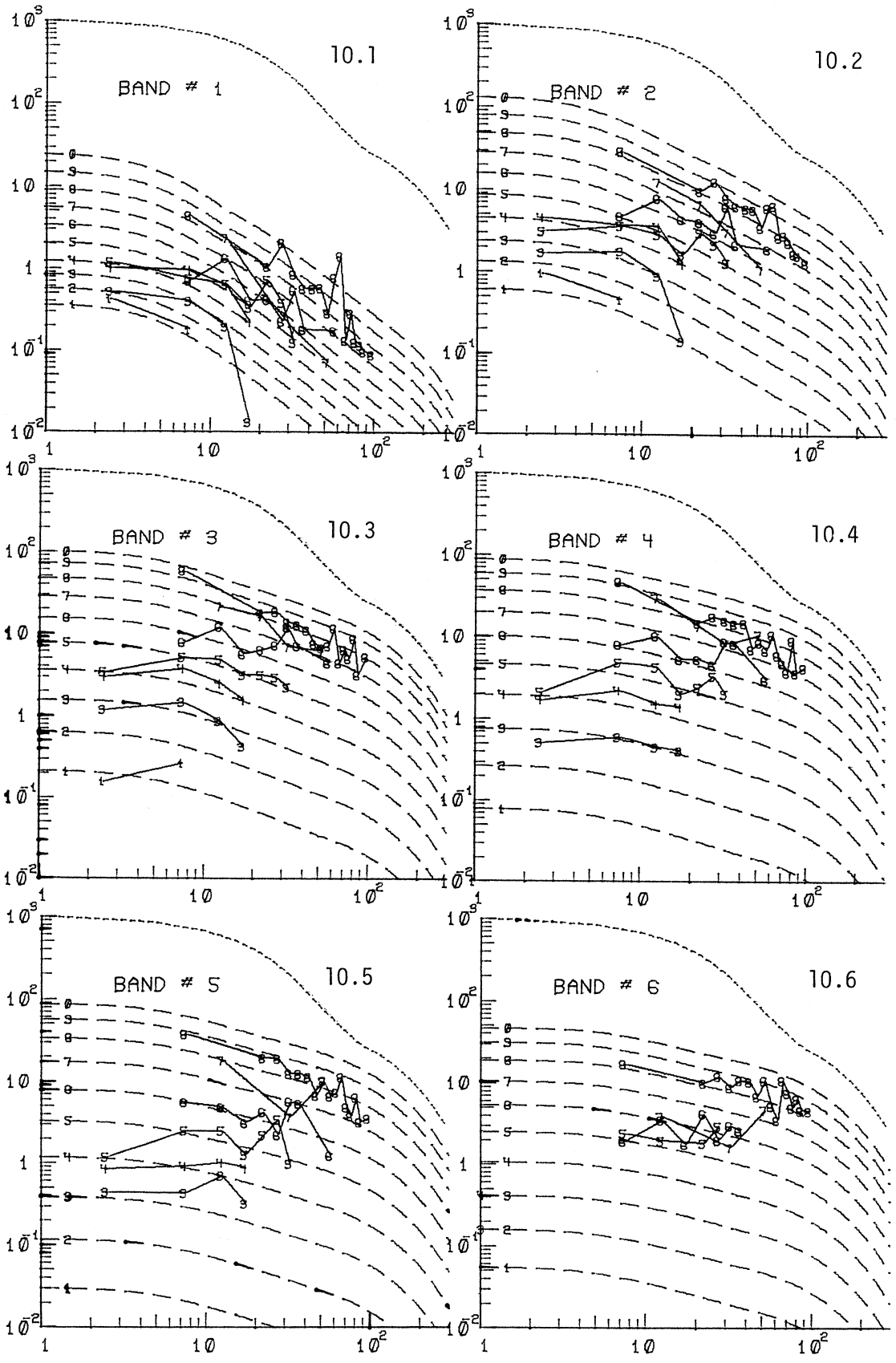

Figures 10.1-10.6 - Average modified FS amplitudes (full irregular lines) for M = 3.5(1), 4.5(2), 5.0(3), 5.5(4)....7.0(8) and 7.9(9) at 6 period bands. Dashed lines represent the corresponding amplitude trends predicted by the regression Model IV. Top dotted line illustrates the shape of $\log_{10} A_o(R)$ attenuation law.

TABLE 10-1

Band #	Range (Sec.)	$S_{6.5}$	C_o
1	.04-.10	12	-1.60186
2	.10-.24	16	-1.18339
3	.24-.65	14	-.794932
4	.65-1.4	11	-.627334
5	1.4-3.2	19	-.655192
6	3.2-8.0	19	-.556734

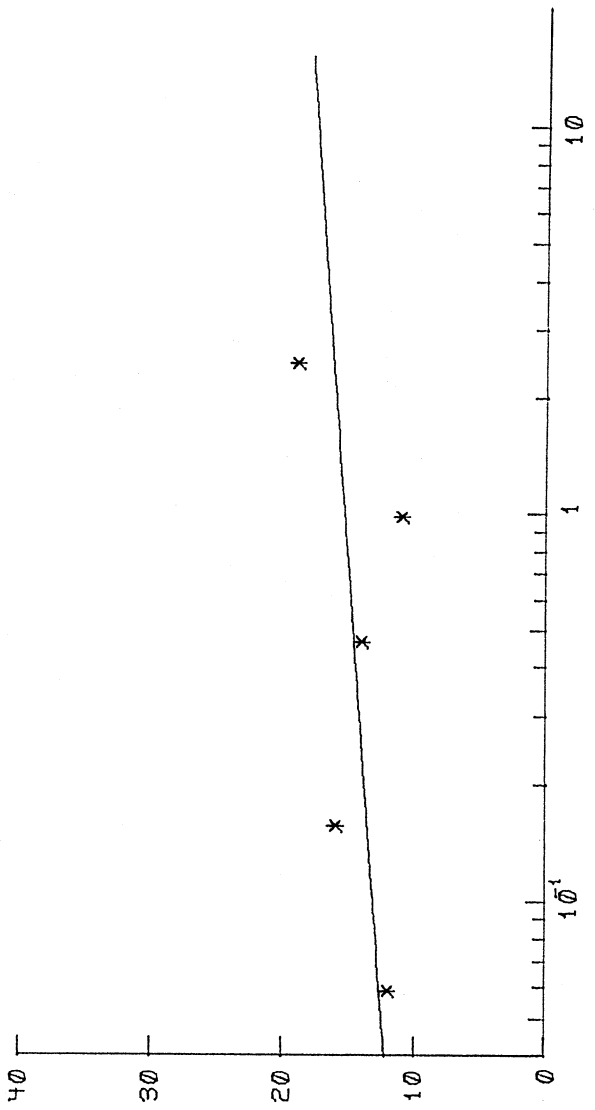

Figure 10.7 - Least Square (Straight Line) Fit of $S_{6.5}$: Model IV.

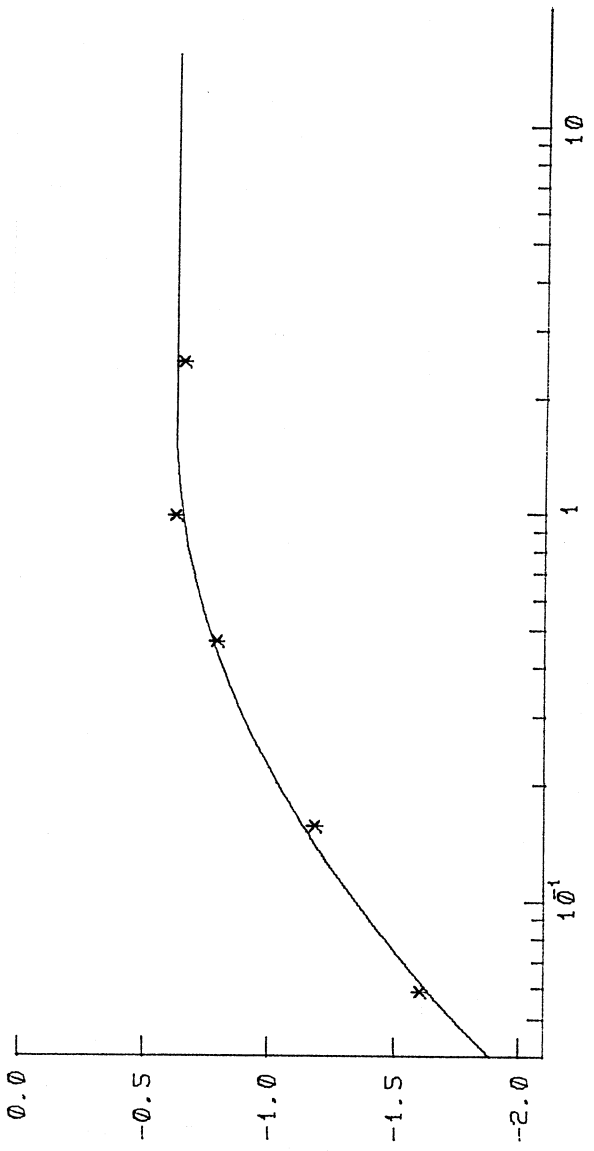

Figure 10.8 - Least Square (Parabolic) Fit of C_o: Model IV.

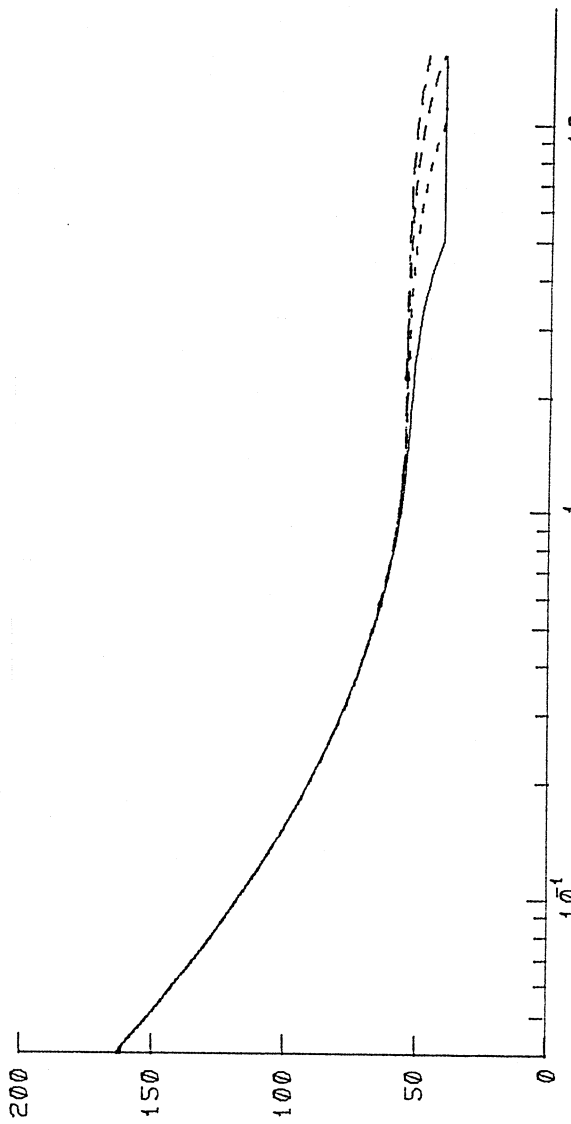

Figure 10.9 - Transition Distances R_o for M = 4, 5, 6, 7: Model IV.

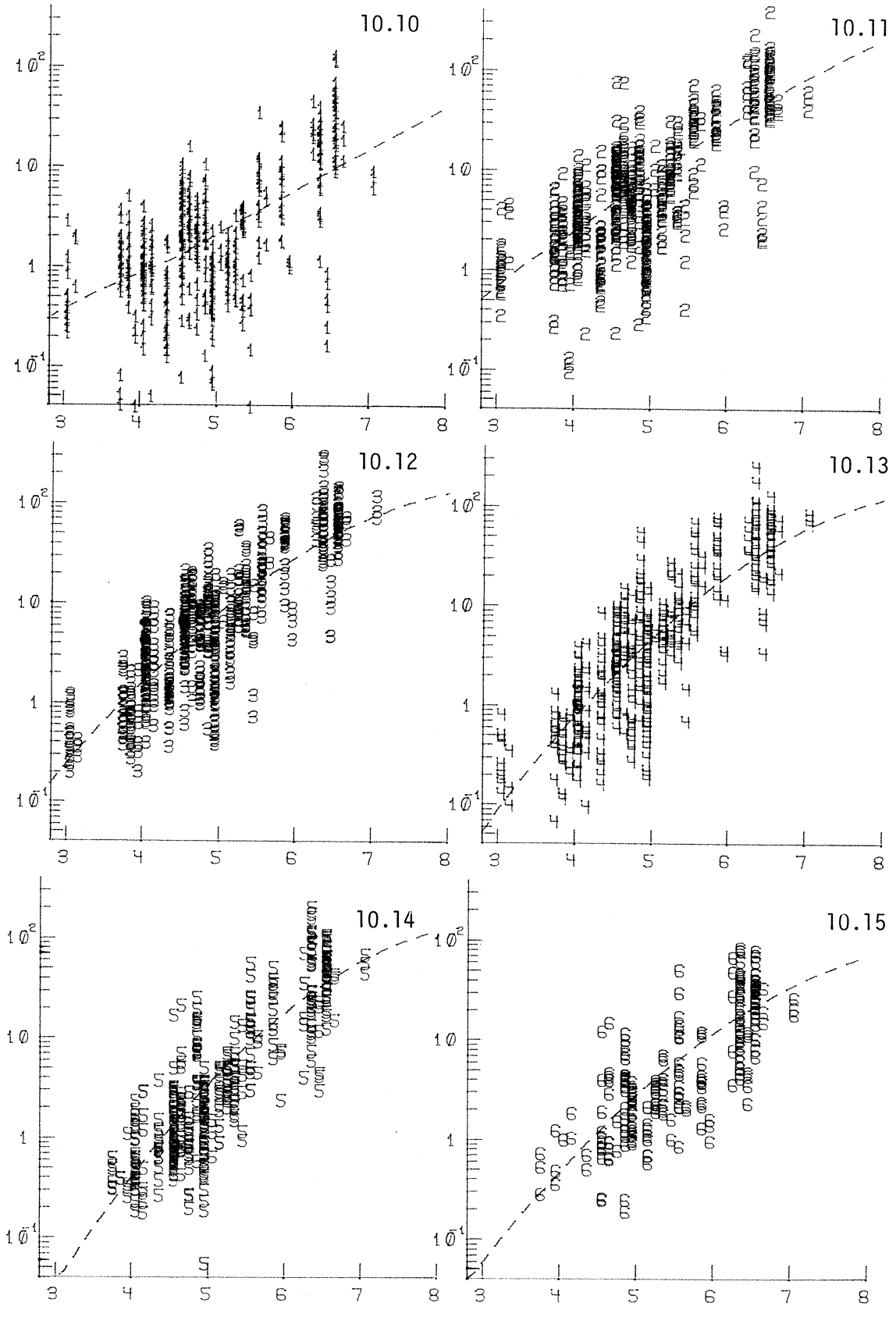

Figures 10-10-10.15 - Estimated (Dashed Lines) and Normalized FS Amplitudes versus M at R = 0 km: Model IV. Arabic numerals indicate the band number.

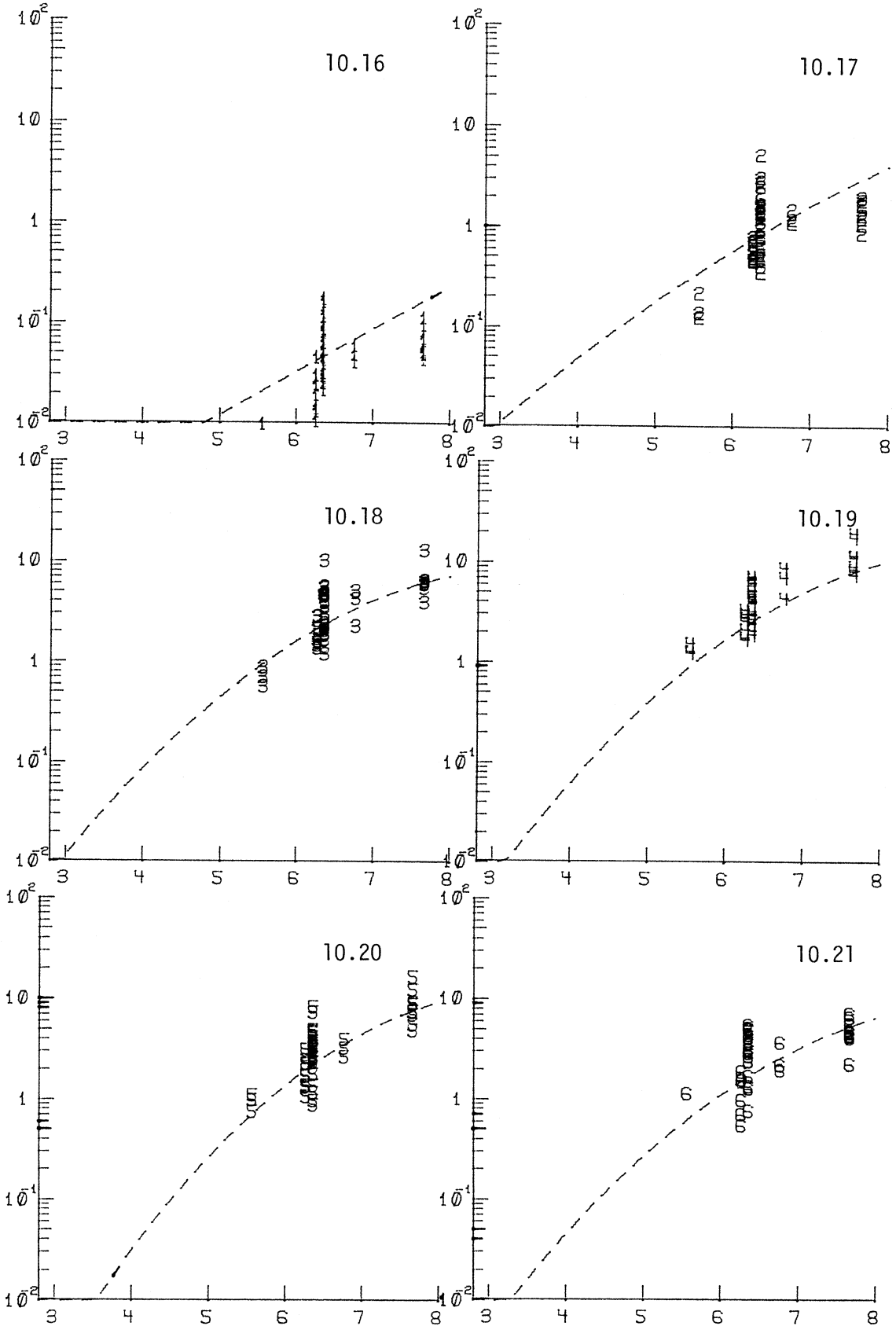

Figures 10.16-10.21 - Estimated (Dashed Lines) and Normalized FS Amplitudes versus M at R = 150 km: Model IV. Arabic numerals indicate the band number.

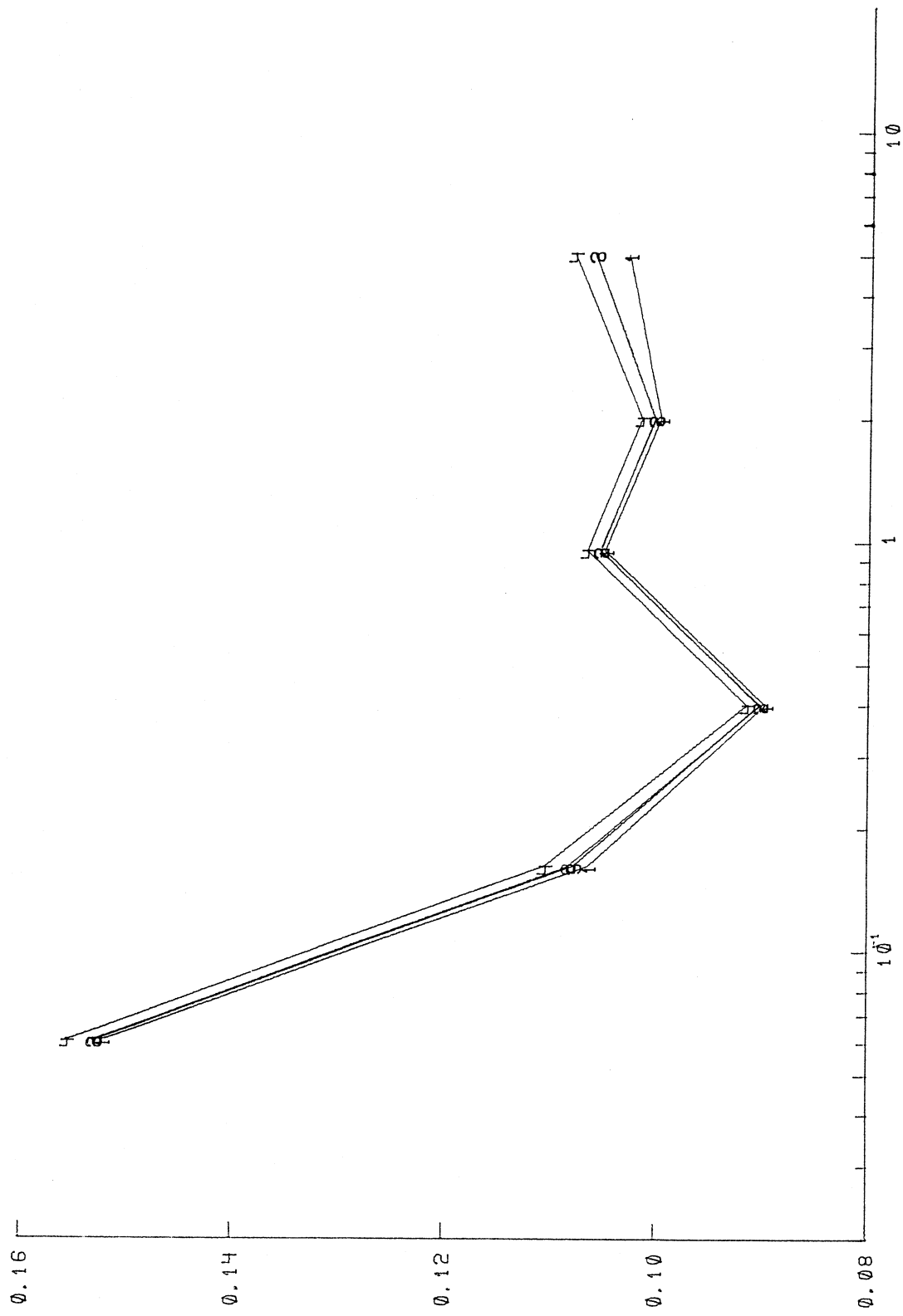

Figure 10.22 - Comparison of the root-mean-squared values of the residues at six bands for four models.

11. Conclusions

The above analysis shows that it is now possible to extract directly from the recorded data, some general frequency and magnitude dependent trends of amplitude attenuation functions with distance. While the data which is available so far is barely adequate to suggest what some of these trends of the attenuation functions might be for distances between about 10 to about 100 km, it is not possible to characterize this attenuation for distances much beyond 100 to 150 km.

For epicentral distances between several kilometers and 100 to 150 km we find clear frequency dependence of Fourier spectrum amplitude attenuation versus distance. Characterizing this dependence by Δ^n, where Δ is the representative distance parameter we find that n ranges from about -0.6 to -0.8 at 0.5 Hz to -1.8 to -2.0 at 20 Hz for the four attenuation models considered. The frequency band No. 6 (periods between 3.2 sec and 8.0 sec), which has been considered throughout this analysis for completeness in presentation, gives smaller n. However, all inferences developed for this frequency band must be taken with caution because this band is influenced by some long period digitization noise, especially for smaller magnitude recordings.

We chose to model the effects of the source size in a crude and simplified manner by adding a characteristic distance (size) S(M,T) to the definition of Δ. We found that the data and our regression analysis do suggest S(M,T) to be increasing with the magnitude to about 20 to 30 km for Model I, to 16 and 20 km for Model II, to 30 km for Model III, and to 10 to 20 km for Model IV at magnitude 6.5.

The magnitudes employed in this work (see Table 3.1) essentially all correspond to the local Richter magnitude, M_L, in southern California. While magnitude determinations of some earthquakes in Table 3.1 have been a subject of more detailed recent investigations (e.g., Imperial Valley earthquake of 1940 (M = 6.7) or Kern County earthquake of 1952 (m = 7.7)) and there is some doubt about what should be the best magnitudes to use in a study of this kind, we continue to prefer the choice of "published" rather than some precisely defined magnitude scales (e.g., Nuttli and Herrmann, 1982). This preference is based on a practical consideration of earthquake catalogues which cannot be "corrected" to represent the data in terms of magnitude scales developed during the recent 5 or 10 years and on the basis of information gathered, 30 to 50 years ago or earlier, during times when the methods, seismological knowledge and standards, as well as the available information were at best very different from those of today. In the future we may reach a stage when all earthquakes will be described by well defined and reproducible magnitude scales, but at present the statistical analyses and the methods used should reflect the quality of the data available so far. By "published" magnitudes above we mean the magnitudes usually presented on the basis of M_L and/or M_S as used in California. Clearly, any effort to use our results outside California will require among other required conversions, that one converts from "published" magnitudes in California to "published" magnitudes as defined and as used in the region of interest.

To employ the new attenuation functions at distances greater than 150 to 200 km it was necessary to extend these functions in some "reasonable" and "physically plausible" way applicable to wave amplitude attenuation in California. We chose to accomplish this by extending the attenuation function at all frequencies by $\log_{10}A_o(R)$ for $R > R_o$ and with $R_o \sim 150$ km at 20 Hz and $R_o \sim 40$ km at ~ 0.2 Hz. It must be emphasized that this represents merely an interim approximation, to facilitate risk calculations at greater distances. At present there is no basis to assume that $\log_{10}A_o(R)$ for $R > R_o$ will continue to be a good choice when more distant strong motion acceleration data becomes available.

We consider four "near field" models of attenuation function. Two (Models I and III) in which the source dimension S(M,T) is "felt" at all epicentral distances including R = 0. The other model (Model II) has S(M,T) multiplied by an exponential function diminishing to zero at R = 0, so that at R = 0 the source size S(M,T) is not "felt" at the recording station, while at $R \sim S(M,T)$, 90% is felt. For Model IV at hypocentral distances smaller than S(M,T), the size of the fault "felt" at the recording station is set equal to the hypocentral distance. This results in Model IV properties being similar to those for Model II.

For Models I and III the rate of growth of spectral amplitudes with magnitude at R = 0 km is small for high frequencies (20 hz) and changes from about 1 at M = 3 to about 3 at M = 7 on an arbitrary amplitude scale. For long periods ($T \sim 5$ sec) the corresponding change in spectral amplitudes is over two orders of magnitude e.g., Figs. 7.15, 8.15, 9.15 and 10.15). For Models II and IV the

rate of growth of spectral amplitudes with magnitude at R = 0 km for high frequencies (20 Hz) is larger than for Models I and III and is closer to the rate of growth for intermediate and long period spectral amplitudes.

Comparison of the residuals of the regression analyses for all four models (equation 10.1 and Figure 10.22) and for all six frequency bands shows that essentially all models fit the data equally well. This means that for modified definitions of S(M,T) for Models II and IV do not change the shapes of the attenuation functions enough for this effect to be detected through the regression analysis in the distance range where most data is available at present, say R > 10 km. This also means that the simple Model I of the "representative" distance $\Delta = (R^2 + H^2 + S^2)^{\frac{1}{2}}$ is capable of portraying all trends in the available data equally well as the Models II, III and IV. (Figure 10.22). Remembering the considerations of the physical processes at the earthquake source, as discussed in the previous sections of this paper and elsewhere (e.g. Gusev, 1983), for the sake of simplicity, and to fit well, the Fourier spectrum amplitudes of the strong motion data which is available so far it would seem that the Model III is the most convenient to use from now on.

In this work we focused onto the analysis of an attenuation function of spectral amplitudes only, and though we did include other scaling parameters (site conditions, vertical versus horizontal components, depth of alluvium) into the regression models used here, we leave detailed presentation on those parameters for another future paper.

12. Acknowledgements

The idea of how to search for the functional form of the attenuation function as studied here, was originated by J. E. Luco during one of our discussions. He also read the paper and offered many useful suggestions and improvements. We are most grateful for his many contributions.

This work was supported in part by a contract from the U.S. Nuclear Regulatory Commission through SEEC and by grants from the National Science Foundation.

REFERENCES

Aki, F. and P. G. Richards (1980) Quantitative Seismology, Freeman and Co., San Francisco.

De Hoop, A. T. (1958) Representation Theorems for the displacement in an elastic solid and their application to elastodynamic diffraction theory, Thesis, Technische Hogeschool, Delft.

Gusev, A. A. (1983) Descriptive statistical model of earthquake source radiation and its application to an estimation of short-period strong motion, Geoph. J. R. Astr. Soc. 74, 787-808.

Gutenberg, B. and C. F. Richter (1942) Earthquake magnitude, intensity, energy and acceleration, Bull. Seism, Soc. Amer., 32, 163-191.

Gutenberg, B. and C. F. Richter (1956) Earthquake magnitude, intensity, energy and acceleration II, Bull. Seism. Soc. Amer., 46, 105-195.

Haskell, N. A. (1969) Elastic displacements in the near-field of a propagating fault, Bull. Seism. Soc. Amer., 59, 865-908.

Hudson, D. E. (1983) Proceedings of the Golden Anniversary Workshop on Strong Motion Seismometry, March 30-31, 1983, Dept. of Civil Eng. Univ. of Southern California, Los Angeles, California.

Nuttli, O. W. and R. H. Herrmann (1981) Ground Motion of Mississippi Valley Earthquakes, ASCE, Oct. 26-31, meeting at St. Louis, Mo.

Nuttli, O. W. and R. H. Herrmann (1982) Earthquake Magnitude Scales, J. of the Geotechnical Division, ASCE, Vol. 108, No. GT5, 783-786.

Richter, C. F. (1958) Elementary Seismology, Freeman, San Francisco.

Trifunac, M. D. (1972) Stress estimates for San Fernando, California, earthquake of February 9, 1971: Main event and thirteen aftershocks, Bull. Seism. Soc. Amer., 62, 721-750.

Trifunac, M. D. (1974) A three-dimensional dislocation model for the San Fernando, California earthquake of February 9, 1971, Bull. Seism. Soc. Amer., 64, 149-172.

Trifunac, M. D. (1976a) Preliminary analysis of the peaks of strong earthquake ground motion - dependence of peaks on earthquake magnitude, epicentral distance, and the recording site conditions, Bull. Seism. Soc. Amer., 66, 189-219.

Trifunac, M. D. (1976b) Preliminary empirical model for scaling Fourier amplitude spectra of strong ground acceleration in terms of earthquake magnitude, source to station distance and recording site conditions, Bull. Seism. Soc. Amer., 66, 1345-1373.

Trifunac, M. D. and A. G. Brady (1975) On the correlation of peak accelerations of strong motion with earthquake magnitude, epicentral distance and site conditions, Proc. U. S. National Conf. on Earthquake Eng., Ann Arbor, Michican, 43-52.

Trifunac, M. D. and J. G. Anderson (1977) Preliminary Empirical Models for Scaling Absolute Acceleration Spectra, Dept. of Civil Eng. Report No. 77-03, Univ. of Southern California, Los Angeles, California.

Trifunac, M. D. and J. G. Anderson (1978a) Preliminary Empirical Models for Scaling Pseudo Relative Velocity Spectra, Dept. of Civil Eng. Report No. 78-04, Univ. of Southern California, Los Angeles, California.

Trifunac, M. D. and J. G. Anderson (1978b) Preliminary Models for Scaling Relative Velocity Spectra, Dept. of Civil Eng. Report No. 78-05, Univ. of Southern California, Los Angeles, California.

Trifunac, M. D. and V. W. Lee (1978) Dependence of the Fourier Amplitude Spectra of Strong Motion Acceleration on the Depth of Sedimentary Deposits, Dept. of Civil Eng. Report No. 78-14, Univ. Southern California, Los Angeles, California.